J. Fluid Mech. (2018), *vol.* 851, *pp.* 50–82.
doi:10.1017/jfm.2018.474

The role of the seam in the swing of a cricket ball

Rahul Deshpande[1,2], Ravi Shakya[1,2] and Sanjay Mittal[1,2,†]

[1]Department of Aerospace Engineering, Indian Institute of Technology Kanpur, UP, India 208016

[2]National Wind Tunnel Facility, Indian Institute of Technology Kanpur, UP, India 208016

(Received 29 August 2017; revised 30 April 2018; accepted 4 June 2018;
first published online 19 July 2018)

The role of the seam in the 'swing' of a cricket ball is investigated via unsteady force and surface-pressure measurements and oil-flow visualization in a low-turbulence wind tunnel. Various seam angles of the ball and flow speeds are considered. Static tests are carried out on a new 'SG Test' cricket ball as well as its idealized models: a smooth sphere with one and five trips. To study the effect of surface roughness of the ball as the game progresses, force measurements are also carried out on a cricket ball that is manually roughened, on one-half and completely, to model a ball that has been in play for approximately 40 overs (240 deliveries/balls). The Reynolds number (Re) is based on the free-stream speed and diameter of the respective model. A new cricket ball experiences three flow states with increase in Re: no swing (NS), conventional swing (CS) and reverse swing (RS). At relatively low Re, in the NS regime, the seam does not have any significant effect on the flow. The separation of the laminar boundary layer, with no subsequent reattachment, is almost axisymmetric with respect to the free-stream flow. Therefore, the ball does not experience any significant lateral force. Beyond a certain Re, the boundary layer on the seam side of the ball undergoes transition. The boundary layer on the non-seam side, however, continues to undergo a laminar separation with no reattachment, thereby creating a lateral force in the direction of the seam, leading to CS. The onset of the CS regime is marked by intermittent formation of a laminar separation bubble (LSB) on the surface of the ball in the region between the laminar separation of the boundary layer and its reattachment at a downstream location. Owing to the varying azimuthal location of the seam, with respect to the front stagnation point on the ball, the transition via LSB formation is localized to a specific region over the seam side. In other regions, the boundary layer either transitions directly without the formation of an LSB, or separates on encountering the seam with no further reattachment. The spatial extent of the region where the flow directly transitions to a turbulent state increases with increase in Re, while that of the LSB decreases. Interestingly, the flow dynamics is such that the magnitude of the swing force coefficient stays relatively constant with increase in Re. With further increase in Re, the boundary layer on the non-seam side undergoes a transition via formation of an LSB. This, along with an upstream shift of the separation point on the seam side, leads to a switch in the direction of the lateral force. It now acts away from the seam, and leads to RS. The transition from CS to RS occurs over a very narrow range of Re wherein the flow intermittently switches between the two flow states. It is observed that the transition of the boundary layer on the seam side leads to an upstream shift of the separation point on the non-seam side at the onset of CS. A complementary effect is observed

† Email address for correspondence: smittal@iitk.ac.in

at the onset of RS. Experiments on a ball that is manually roughened bring out the relative effect of the seam and roughness on the transition of the boundary layer. Compared to a new ball, the magnitude of the maximum swing force coefficient for a rough ball is smaller during the CS regime, and larger during the RS regime. Unlike other models, the ball with roughened non-seam side and smooth seam side, for certain seam orientations, exhibits RS at relatively lower speeds and CS at higher speeds. The forces measured on the cricket ball are utilized to estimate the trajectory of the ball bowled at various initial speeds and seam angles. The lateral movement of the ball depends very significantly on the seam angle, surface roughness and speed of the ball at its delivery. The maximum lateral deviation of a new ball during RS is found to be less than half of that observed in CS. On the other hand, the lateral movement of a roughened ball during RS may significantly exceed its movement during CS. The range of the speed of the ball, for various seam orientations and surface roughnesses, are estimated wherein it undergoes CS, RS or one followed by the other. Optimal conditions are estimated for the desired lateral movement of the ball.

Key words: boundary layers, boundary layer separation, wakes

1. Introduction

Cricket is a popular bat-and-ball sport. The cricket ball is an assembly of two hemispheres that are held together by prominent stitches which form a 'seam' (see figure 1). One of the tactics employed by the bowler, to deceive the batsman, is controlling the lateral movement of the ball during its flight. The physics associated with the 'swing' of the ball has received considerable attention in the past (Barton 1982; Bentley *et al.* 1982; Sherwin & Sproston 1982; Mehta *et al.* 1983) and continues to be of interest. The interested reader can refer to the article by Mehta (1985) for a comprehensive review on this subject.

The flow past a smooth sphere, which forms the primary building block for understanding the flow past a cricket ball, has been studied in fair detail in the past. One of the most comprehensive studies on the various flow states observed for a smooth sphere was carried out by Achenbach (1972). The variation of the mean drag coefficient ($\overline{C}_D$) with *Re* was investigated and utilized to classify the flow in four regimes: subcritical, critical, supercritical and transcritical. The Reynolds number, *Re*, is based on the free-stream speed of the flow and the diameter of the sphere. Within the critical regime, the transition of the boundary layer and the formation of a laminar separation bubble (LSB) cause a very substantial reduction in the drag on a sphere (Achenbach 1972; Singh & Mittal 2005). Deshpande *et al.* (2017) found that the LSB forms intermittently in the initial stages of transition. They proposed that the critical flow regime can be further classified into three subregimes on the basis of the nature of the LSB. The $\overline{C}_D$ value increases gradually with increase in *Re* in the supercritical and transcritical regimes. The location of the boundary layer transition moves upstream.

The time-averaged flow past a stationary smooth sphere, in the *Re* regime corresponding to the swing of a cricket ball, is largely axisymmetric (Deshpande *et al.* 2017). The asymmetries due to the minute manufacturing imperfections on the surface of the sphere (Norman & McKeon 2011) are not sufficient to explain the

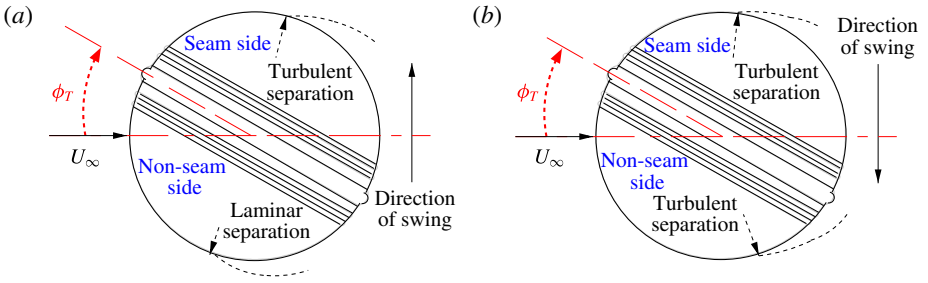

FIGURE 1. (Colour online) Schematic of the flow past a cricket ball for (*a*) conventional swing (CS) and (*b*) reverse swing (RS). The ball is travelling from right to left, so air flow relative to the ball with speed U_∞ is as shown.

swing of the cricket ball. Some of the possible mechanisms that can alter the basic flow past a sphere to generate the lateral force on a cricket ball are: (i) the seam, oriented at an angle to the free stream, which may act as a boundary layer trip (Mehta 1985); (ii) differential roughness of the surface of the ball (Mehta 2014) on the seam and non-seam sides (figure 1 shows a schematic of the seam and non-seam sides); and (iii) rotation of the ball due to the backspin imparted to it by the bowler at the time of delivery (Mehta 2014). Earlier studies (Achenbach 1974; Son *et al.* 2010, 2011; Kim *et al.* 2014) have shown that the primary effect of such boundary layer perturbations, on the flow over a sphere, is the shifting of the drag crisis to a lower *Re*. More importantly, the formation of an LSB remains the primary mechanism behind the drag reduction, even in presence of the boundary layer perturbations. We briefly discuss each of the three mechanisms.

The seam oriented at an angle to the incoming flow renders asymmetry to the flow past the ball, resulting in a lateral movement during its flight, which may be significant under certain conditions. The swing is of one of two types: conventional swing (CS) and reverse swing (RS). Figure 1 shows a schematic of the flow around the ball for the two types of swing. The swing of the ball is an outcome of the pressure asymmetry between its seam and non-seam sides (Mehta *et al.* 1983; Mehta 1985). During CS, the seam causes the laminar boundary layer, on the seam side of the ball, to transition to a turbulent state (Mehta *et al.* 1983), thereby significantly delaying the flow separation. The boundary layer over the non-seam side remains laminar and separates upstream of the shoulder of the ball. This results in relatively greater suction on the seam side, leading to a lateral force towards this side of the ball (Mehta *et al.* 1983). It also causes tilting of the near wake, towards the non-seam side of the ball (figure 1*a*). In a strict sense, the term 'swing' refers to the lateral movement of the ball. However, in the bulk of this article, it is used interchangeably with 'swing force' acting on the ball. Later in the article, the term 'swing' is used in its conventional sense to discuss the trajectory of the ball.

At a certain threshold speed, which corresponds to the critical Reynolds number for the natural transition of the boundary layer on the non-seam side, the flow separation is delayed on this side as well, reducing the flow asymmetry. The flow, however, continues to be in the CS regime. According to Mehta (2005), a further increase in *Re* results in the upstream movement of the boundary layer transition and separation points on both sides. When the transition location on the seam side moves upstream of the seam, the turbulent boundary layer 'thickens' on encountering the seam. Such a boundary layer tends to separate at a relatively early azimuthal location compared

to the 'thinner' turbulent boundary layer over the non-seam side. This creates a higher suction on the non-seam side as compared to that on the seam side, resulting in a net force towards the non-seam side of the ball. The ball undergoes RS as a result of this force. The near wake, in this flow regime, tilts towards the seam side (figure 1*b*). It was shown by Mehta (2005) that, in contrast to the popular belief, a new cricket ball can also undergo RS, albeit at relatively higher speeds.

The cricket ball wears out during play; the surface becomes rougher and the seam less pronounced (Mehta 2014). In the initial stage of a game, when the roughness is not very significant, the seam plays the key role in the swing of the ball. As the game progresses, the bowling team maintains the polish over one half of the ball using sweat/saliva while allowing the other to roughen naturally (Mehta 2005). With significant roughening of one half and deterioration of the seam, the contrasting surface roughness between the two halves is the key to achieving swing (Mehta 2014). Differential boundary layer growth due to contrasting surface roughness on the two sides of the ball creates pressure asymmetry on the two sides. The swing of the ball via this mechanism is referred to as contrast swing (Mehta 2014). The bowler can utilize the seam orientation, just as for a new ball, to control the movement of the ball due to contrast swing. The swing of a roughened cricket ball, and its comparison with that of a new one, is investigated in this work.

Kim *et al.* (2014) showed that a spinning sphere may also experience a lateral force due to the pressure differential on the 'advancing' and 'retreating' sides. The force can be towards the retreating side due to the Magnus effect or the advancing side because of the inverse Magnus effect. In either case, the force due to the rotation is restricted to the plane of the rotation of the sphere. Most cricket bowlers, intending to swing the ball, release it along the seam (Mehta 1985). Except for the bowlers with a side-arm action, the axis of the backspin of the ball at its release is close to horizontal and normal to the plane of the seam. The primary force on the ball due to rotation is therefore either vertically upwards due to the Magnus effect or downwards because of the inverse Magnus effect. The swing force, on the other hand, acts sideways in a direction that is almost normal to the plane containing the seam of the ball. Therefore, the pressure asymmetry generated due to the Magnus/inverse Magnus effect is not expected to directly contribute to the lateral movement of the ball. Barton (1982), however, showed that the swing force on the ball is actually affected by the rotation of the ball; its magnitude decreases with increase in rotation rate. He argued that the rotation 'activates' the irregularities of the ball, such as its non-sphericity, embossment marks, etc., on the surface of the ball. Therefore, the boundary layer is perturbed not just by the seam, but also due to these effects. The primary objective of the present study is to understand the role of the seam on the swing of a cricket ball. Therefore, the effect of rotation of the ball is not explored in this work. All experiments are conducted for flow past a non-spinning cricket ball and its simplified models.

There have been relatively few efforts in the past to investigate the effect of a trip on the flow past a sphere (Wieselsberger 1914; Maxworthy 1969; Son *et al.* 2011). In addition, in none of these studies does the placement of the trip resemble the seam of a cricket ball. For example, in the study conducted by Son *et al.* (2011), the trip wire traces a circle on the sphere where each point on it is at the same azimuthal angle, with respect to the front stagnation point of the sphere, such that the incoming flow sees an axisymmetric set-up. They found that the transition of the boundary layer can occur in one of two ways depending on the size of the trip. If the trip is smaller than the thickness of the boundary layer, the disturbance due to the trip causes a delayed laminar separation, close to the shoulder of the sphere. Thereafter,

the separated shear layer transitions to a turbulent state, resulting in the reattachment of flow and formation of a secondary separation bubble. On the other hand, if the trip is larger than the thickness of the boundary layer, it produces disturbances that are significant enough to cause flow separation, transition and reattachment immediately downstream of the trip. Igarashi (1986) conducted a similar set of experiments for a circular cylinder. Depending on the *Re* of the flow and the size and location of the trip, it was found that the flow downstream of the trip may either: (i) relaminarize; (ii) transition to a turbulent state and reattach as a turbulent boundary layer; or (iii) remain separated with no further reattachment. The effect of surface roughness on the transition of the boundary layer, in flow past a sphere, was investigated by Achenbach (1974). Increased roughness leads to an earlier transition. In addition, the LSB for a rough sphere is observed during a relatively smaller range of *Re* as compared to that for a smooth sphere. Beyond the transition, a rough sphere is associated with wider wake and a higher coefficient of drag.

Despite a fairly large number of studies in the past that have addressed the phenomenon of the swing of a cricket ball, there are gaps in the understanding of the role of seam in generating CS and RS. Most studies have focused on the influence of the rotation rate, surface roughness, seam angle and other aspects of the geometry of the ball on swing. The study by Scobie *et al.* (2012) brings out important aspects related to the flow physics of no swing (NS), CS and RS. For a scaled model of a new cricket ball in the regime of RS, they observed an LSB on the non-seam side. However, their study brings out the structure of flow neither in the regime of CS nor during the transition from CS to RS, motivating further exploration.

The objective of the present study is to investigate the mechanism of conventional and reverse swing for a new as well as a used/rough cricket ball. Specifically, we attempt to address the following five questions. (1) How does the coefficient of swing force vary with *Re* for a new as well as a rough ball? (2) What is the structure of the flow during conventional and reverse swing, and during the transition between flow regimes? (3) During CS, does the boundary layer trip to a turbulent state immediately downstream of the seam at all polar angles on encountering it? (4) How does the spatial location and size of the LSB on the seam and non-seam sides change with *Re* in various regimes? (5) Can the force measurements be utilized to predict the lateral movement of the ball? To this end, experiments are carried out in a low-turbulence wind tunnel on a new as well as a rough cricket ball and its scaled models. Owing to the manufacturing process, there are minor variations in the geometry and surface roughness between different specimens of the ball. Therefore, to understand the role of the seam, idealized models of the cricket ball are considered. These are smooth spheres with trip wires that mimic the effect of the seam of the cricket ball. Unsteady force and surface-pressure measurements and oil-flow visualization are conducted. The trajectory of the ball, delivered at various speeds and seam orientations, is estimated by integrating the equation of motion and utilizing the forces measured from wind-tunnel experiments on the cricket ball.

2. Experimental set-up

The experiments were conducted in a closed-circuit suction-type atmospheric wind tunnel with a test section size of 3 m $\times$ 2.25 m. The maximum achievable wind speed in the test section is 80 m s^{-1}. The maximum spatial inhomogeneity of the incoming flow was measured to be approximately 0.05 % at a speed of 20 m s^{-1}. The turbulence intensity in the tunnel test section was measured to be

Model type	Diameter (mm)	Seam angles (ϕ_T) studied	Trip height-to-diameter ratio	Measurements carried out	Sting-to-model diameter ratio
Smooth sphere	120 (D_1)	—	—	Force and oil-flow vis.	0.075
'SG Test' cricket ball	71 (approx.)	10°, 20° and 30°	0.0141	Force	0.127
Sphere with five trips	71 (D_3)	30°	0.0141	Force and oil-flow vis.	0.127
Sphere with one trip	110 (D_2)	30°	0.0150	Force, oil-flow vis. and surface press.	0.082 0.191

TABLE 1. A summary of the experimental studies conducted on various sphere/ball configurations. The ratio of the trip height to diameter of the sphere is for the tallest trip in the case of models with multiple trips.

below 0.06 % throughout the operating speed range of the tunnel. More details on the characterization of the wind tunnel can be found in the article by Cadot *et al.* (2015). The measurements in the present study were carried out in the velocity range 10–75 m s^{-1}.

Experiments have been carried out with a real cricket ball as well as three models of a sphere. The models as well as the schematic of their mounting are shown in figure 2. Some details of the models as well as the measurements carried out using them are listed in table 1. Owing to the limitations of the available instrumentation and set-up, some of the measurements for certain models, such as oil-flow visualization, force and surface-pressure measurements, could not be carried out simultaneously and were done in separate runs.

Wind-tunnel tests were first carried out on a smooth sphere to validate the experimental set-up shown in figure 2. Next, tests were carried out on new as well as rough 'SG Test' cricket balls, which are the balls used in international test cricket matches played in India. Figure 3 shows a new cricket ball mounted in the test section of the wind tunnel, for force measurements. Experiments have been carried out for a cricket ball with its seam oriented at different angles to the incoming flow (table 1). Figure 2 shows the definition of the trip/seam angle, ϕ_T. Also shown in the figure is the polar angle θ, which is used later in the paper to show the variation of certain quantities on the surface of the sphere. To realize a certain seam orientation, a hole needs to be drilled on the ball for its mounting on the sting. It was found that one single specimen is unable to sustain too many holes. Therefore, two balls were used: one for $\phi_T = 10°$ and 30°, and the other for $\phi_T = 20°$.

One of the objectives of the present work is to study the effect of surface roughness of the ball. A 40-overs-old (240 deliveries) ball is considered sufficiently rough to influence the transition of the boundary layer. The cricket team of our Institute was contacted to decide on the specimen for experiments on rough balls. A large number of cricket balls, used in cricket matches for 15–40 overs, were inspected. It was found that, in general, as the match progresses the ball becomes not only rougher but also deforms to being more non-spherical. To enable studying the effect of surface roughness, while not adding complexity due to deformation, it was decided to manually roughen a new ball using sandpaper instead of testing an actual used ball. Following several trials, a 60-grit sandpaper was found to be appropriate to introduce roughness equivalent to a 40-overs-old ball. Three cases of a roughened ball are

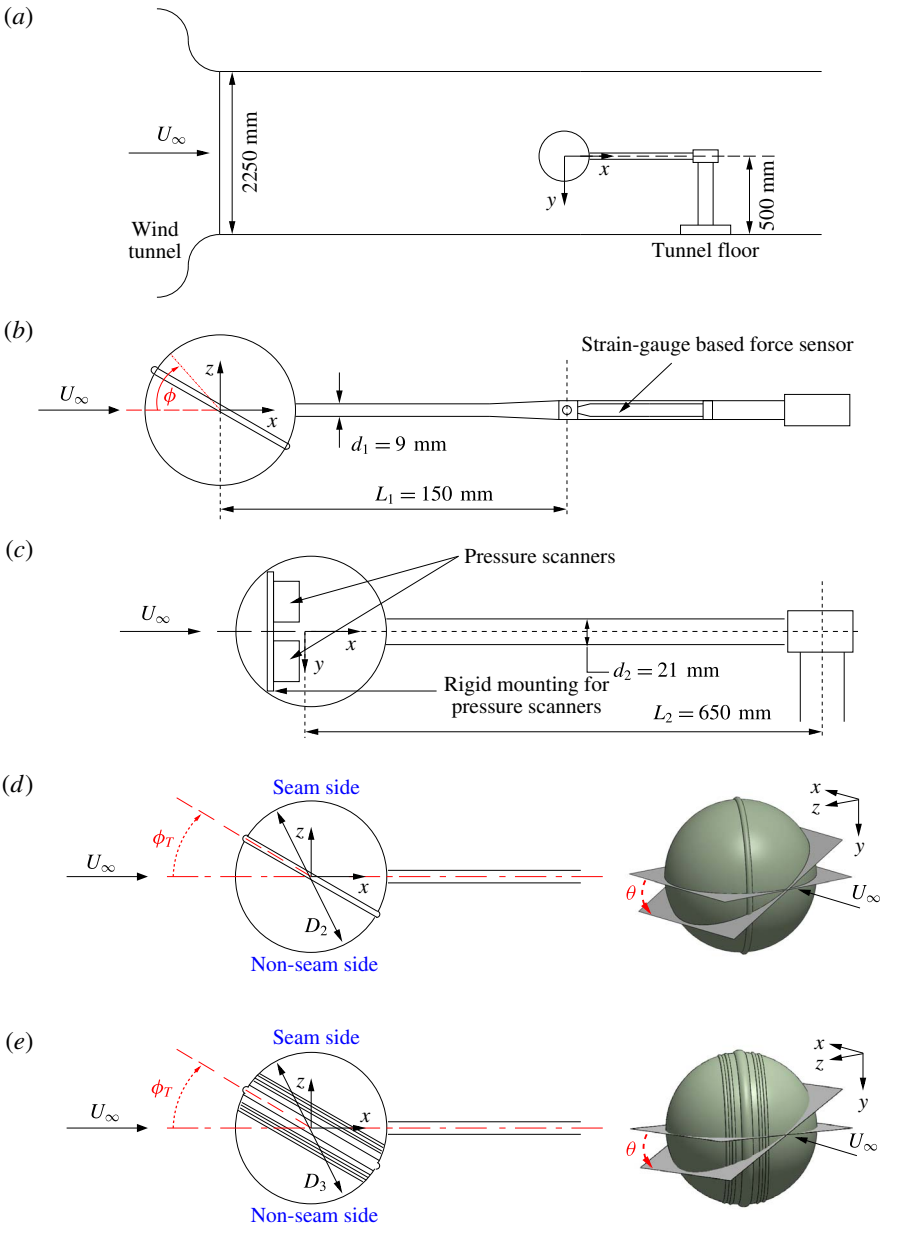

FIGURE 2. (Colour online) (*a*) Schematic of the model mounting in the tunnel test section (dimensions are in millimetres) along with the coordinate axes. The set-up for force and surface-pressure measurements are shown in (*b*) and (*c*), respectively. Panels (*d*) and (*e*), respectively, show the mounting of the sphere with one trip and sphere with five trips models along with the definition of the various angles. Angle ϕ is the azimuthal angle, with respect to the front stagnation point, while θ is the polar angle. The inclination of the trip/seam to the incoming flow direction is indicated by ϕ_T.

tested for each seam orientation. (i) S–R: the half of the ball that is relatively rough by default, due to the manufacturer's embossments, is roughened and oriented so that

FIGURE 3. (Colour online) An SG Test cricket ball shown mounted on the experimental set-up in the wind-tunnel test section.

the seam side is rough while the non-seam side is 'shiny'. (ii) NS–R: the same ball as in (i) is reoriented so that the non-seam side is the rough one while the seam side is 'shiny'. Both cases are candidates that may lead to 'contrast swing'. (iii) C–R: the entire ball is roughened. In all three cases, the seam is also roughened.

To further understand the role of the seam of the cricket ball, experiments were conducted on two models of smooth spheres with trip(s). One of the models, with five trips on its surface (figure 2*e*), is similar to a new SG Test cricket ball. There is only one trip, along a plane of symmetry, on the other model (figure 2*d*). We refer to these models as sphere with five trips and sphere with one trip, respectively. The diameter of each of the models, listed in table 1, was selected to ensure that the transition of the boundary layer occurs within the operating range of the wind tunnel. According to Son *et al.* (2011), the ratio of boundary layer thickness to the diameter of the sphere, at $\phi = 80°$, is 0.0045 at $Re = 10^5$. The height of the tallest trip for the sphere-with-trip(s) models, in the present study, is greater than the estimated boundary layer thickness at that location for the range of Re explored in this study (table 1).

The blockage ratio of the cross-sectional area of the largest model (smooth sphere) to the area of the test section is approximately 0.16 %. All the models were 3D-printed using the selective laser sintering technique with nylon PA 12 material. The geometry of the trips was embedded in the manufacturing drawings. The fabrication resulted in a good surface finish corresponding to $k/D \approx 83.33 \times 10^{-5}$, where D represents the diameter of the respective sphere model. A paint with matte finish was applied on the model to further improve its surface finish. Each model is an assembly of two hollow pieces that join together, as a tight fit, at an azimuthal angle of $\phi = 130°$ from the front stagnation point. This ensures that the very small gap in the assembly of the two parts is located away from the region of the transition boundary layer. Therefore, it is expected to have no significant influence on the flow. The models were mounted on a horizontal sting fixed to a rigid vertical support, which in turn was anchored to the floor of the test section (figure 2*a*). The sting-to-model diameter ratio (d/D) is below 0.25 (table 1) for all experiments and is in accordance with the suggestion of Norman & McKeon (2008).

A six-component, strain-gauge-based, force sensor was used to measure unsteady forces on the model. The calibration curve obtained for the sensor is linear. The downstream end of the horizontal sting was connected to the sensor. The measurements from the force sensor were corrected for the contribution to the forces due to the sting. The experimental set-up as well as the technique for correction is similar to that used by Suryanarayana, Pauer & Meier (1993). At each Re, 60 s

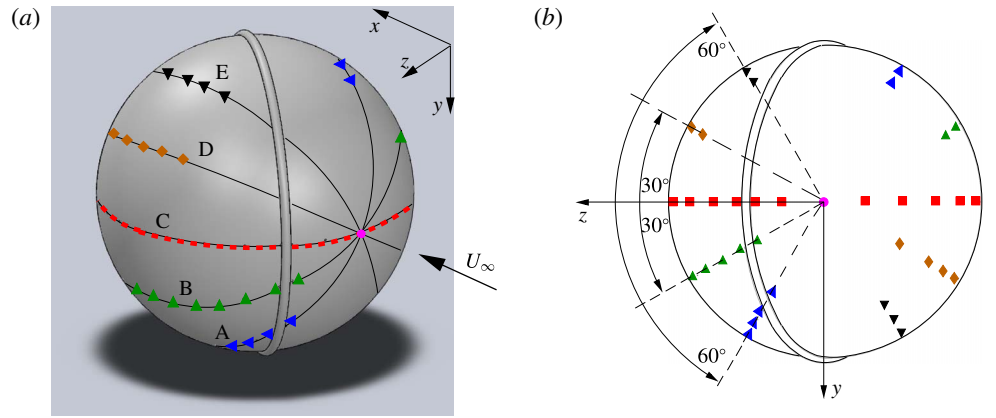

FIGURE 4. (Colour online) Schematic of the sphere-with-one-trip model with pressure ports arranged along five circumferential lines: A (◀), B (▲), C (■), D (◆) and E (▼). The flow is along the positive x-direction and the front stagnation point is shown by a solid circle (●). The size and number of ports shown in the figure are only representative. Not all ports have been shown, to avoid clutter. The origin of the coordinate axes is located at the centre of the sphere model. It has been shifted in (a) for ease of illustrating the orientation of the model.

of data were acquired from the balance at a rate of 500 Hz, and amplified for higher accuracy. The maximum uncertainty in the measurement of drag is estimated to be $\pm 0.2\,\%$. The non-dimensional time (tU_∞/D) for acquisition of data for the lowest flow speed of 10 m s^{-1} is 5000. This is well above the recommended time of 2000 units suggested by Norman & McKeon (2011). In the range of Re where the drag/lateral force was observed to be intermittent between two flow states, force as well as surface-pressure data were acquired for a longer duration of 300 s. The force measurements were repeated at least twice, at each Re. The results from the three runs are in excellent agreement.

Two different sphere-with-one-trip models were fabricated: one with pressure ports on its surface and the other without pressure ports. The model with no pressure ports was used in the oil-flow visualization. Force measurements were conducted on both the models. A total of 108 pressure ports were distributed on the surface of the model. Figure 4 shows their distribution. The holes for the pressure ports were drilled normal to the surface of the model. They are arranged along five circumferential lines named as A, B, C, D and E and shown in figure 4. Such an arrangement of ports provides azimuthal (ϕ) as well as polar (θ) variation of the surface pressure. Table 2 gives the details of the distribution of the ports. As far as possible the ports are symmetrically distributed about the x–y plane so that the asymmetry in the flow is induced primarily by the seam, and not the ports. An additional port at $\phi = 0°$ is used for measuring the stagnation pressure. Four ports were also provided near the upstream end of the horizontal sting, close to $\phi = 180°$, for measurement of back-pressure. The back-pressure reported in this article is the average of the values from these four ports.

Three ESP scanners, each with an operational range of -2500 to $+2500$ Pa, were used for the present study. Two of these were installed on a firm support inside the sphere (figure 2c). They were used to acquire the instantaneous pressure data from the ports on the surface of the model. Accordingly, the pressure measurements required

Circumferential line	Polar angle θ (deg.)	No. of ports on non-seam side	No. of ports on seam side	Azimuthal distribution of ports on seam side
A	60	6	10	$46^\circ \leqslant \phi \leqslant 135^\circ$
B	30	6	11	$31^\circ \leqslant \phi \leqslant 135^\circ$
C	0	21	22	$15^\circ \leqslant \phi \leqslant 155^\circ$
D	−30	10	6	$75^\circ \leqslant \phi \leqslant 125^\circ$
E	−60	9	6	$75^\circ \leqslant \phi \leqslant 125^\circ$

TABLE 2. Distribution of the pressure ports on each circumferential line on the sphere with one trip.

a larger sting diameter to enable the passage of the power supply cables of these pressure scanners (figure 2). One scanner was utilized to acquire the static and total pressure in the tunnel and the back-pressure data on the model. This scanner was kept outside the tunnel. The resolution of the pressure transducer is $\pm 0.05\,\%$ of 2500 Pa. The output signal was sampled for 120 s with an acquisition rate of 500 Hz per pressure port.

Surface oil-flow visualization for the various models was carried out at several free-stream speeds using a mixture of paraffin oil and titanium dioxide. Two cameras were installed outside the tunnel to capture pictures in the x–z and x–y planes. The pictures in the x–z plane bring out the asymmetry in the flow between the seam and non-seam sides of the model, while those in the x–y plane highlight the flow structures on both sides of the model. Further details regarding the set-up for pressure measurements and oil-flow visualization may be found in Deshpande *et al.* (2017).

3. Results

3.1. *Flow past a smooth sphere*

Wind-tunnel tests were first carried out on a smooth sphere to validate the experimental set-up. These measurements also provide base data to analyse the results from the experiments on a cricket ball and sphere with trip(s). Figure 5(*a*) shows the variation of mean drag coefficient, $\overline{C}_D$, for a smooth sphere with Re from the present and earlier studies. The results from the present study are in reasonable agreement with those reported earlier except in the subcritical regime where the current $\overline{C}_D$ is slightly lower than the measurements of Achenbach (1972) and Norman *et al.* (2011). Deshpande *et al.* (2017) made a similar observation and attributed the variation to the difference in experimental set-ups in the studies. We utilize the same set-up as for the smooth sphere, to investigate the flow past a cricket ball and sphere with trip(s).

Oil-flow visualization was also carried out to explore the surface flow phenomena over a smooth sphere (figure 5*b*,*c*). The images enable visualization of flow structures close to the surface of the model and estimation of the azimuthal angles of flow separation and/or reattachment. The three-dimensionality of the flow and the influence of gravity lead to uncertainties in the estimated angles that may be as large as 10° (Taneda 1978; Suryanarayana & Prabhu 2000). Figure 5(*b*) shows the flow in the subcritical regime. The laminar boundary layer separates upstream of the shoulder of the sphere, at $\phi \approx 80^\circ$. The oil upstream of the separation is pushed downstream, leaving a very clear signature of the line of separation. No reattachment of the separated flow is observed in this subregime. Figure 5(*c*) shows the flow in the supercritical regime. In contrast to the flow in the subcritical regime, the laminar

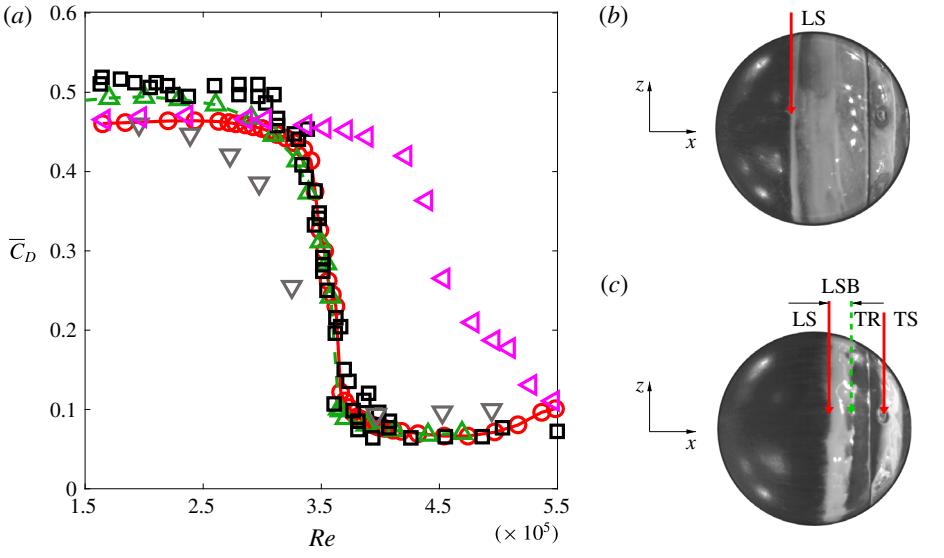

FIGURE 5. (Colour online) Flow past a smooth sphere. (*a*) Variation of the mean drag coefficient with *Re*: ○, present study; □, Achenbach (1972); △, Norman, Kerrigan & McKeon (2011); ▽, Wieselsberger (1922); ◁, Suryanarayana *et al.* (1993). Surface oil-flow patterns for (*b*) subcritical regime ($Re = 1.88 \times 10^5$) and (*c*) supercritical regime ($Re = 4.28 \times 10^5$). LS, TR and TS indicate laminar separation, turbulent reattachment and turbulent separation, respectively.

separation (LS) occurs slightly downstream of the shoulder ($\phi \approx 105°$) and undergoes a turbulent reattachment (TR) at $\phi \approx 120°$. The turbulent boundary layer separates at $\phi \approx 135°$. As a result, an LSB that is bounded by LS and TR is seen in figure 5(*c*) with very distinct boundaries. The oil-flow patterns observed in this study are in good agreement with those reported in earlier flow visualization experiments (Taneda 1978; Suryanarayana & Prabhu 2000).

3.2. *Flow past a new cricket ball*

Figure 6 shows the variation, with *Re*, of the coefficients of the three components of force acting on a new SG Test cricket ball measured in the present study. The seam is oriented at an angle of $\phi_T = 30°$ to the free-stream flow. Unlike the smooth sphere, the new cricket ball, owing to the presence of its seam, experiences a significant lateral force along the z-axis for the entire range of *Re* shown in the figure. The $\overline{C}_Z$ value gradually increases with increase in *Re* up to $Re \approx 1.2 \times 10^5$. It remains nearly constant ($\sim$0.35), up to $Re \approx 1.8 \times 10^5$. This force leads to a lateral movement of the ball in the direction of the seam. It corresponds to conventional swing (CS). At $Re \sim 1.8 \times 10^5$, there is a switch in the direction of the lateral force. For larger *Re*, $\overline{C}_Z$ is approximately -0.15. Such a force is expected to lead to a lateral movement of the ball away from the seam and is referred to as RS. The regimes of conventional and reverse swing, for the present study, are marked in figure 6. Since $\overline{C}_Y$ is rather small for the range of *Re* considered in this work, it is not explored any further in this study. Also shown in figure 6 are measurements for $\overline{C}_D$ and $\overline{C}_Z$ from Sherwin & Sproston (1982) for a non-spinning, new cricket ball at the same seam angle. Their

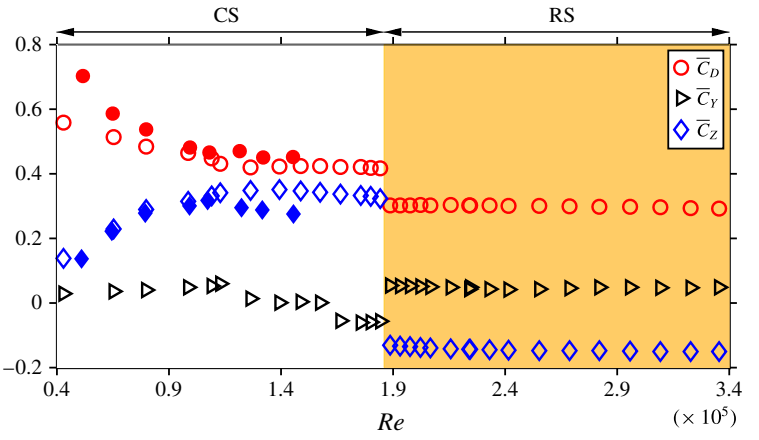

FIGURE 6. (Colour online) Flow past a new cricket ball with $\phi_T = 30°$: variation of the aerodynamic force coefficients with Re. The measurements from the present study are shown in hollow symbols, while those from the study by Sherwin & Sproston (1982) are shown with filled symbols. The Re ranges for CS and RS, corresponding to the present study, are marked and also highlighted via background colour.

study, however, is restricted to $Re \approx 1.5 \times 10^5$. For this range of Re, the variation of $\overline{C}_Z$ from their study and the present one are in good agreement.

A gradual decrease in $\overline{C}_D$ is observed for $0.4 \times 10^5 < Re < 1.2 \times 10^5$ as $\overline{C}_Z$ builds up during CS (figure 6). This is a consequence of the transition of the boundary layer on the seam side while the boundary layer on the non-seam side remains laminar (Mehta *et al.* 1983). Overall, the results from the present study and those from Sherwin & Sproston (1982) are in good agreement. The magnitude of $\overline{C}_D$ reported by Sherwin & Sproston (1982), for the lower range of Re, is slightly larger than that observed in the present study. This may be attributed to the difference in the experimental set-up and the brand of cricket balls used in the two studies. Mehta (2005) proposed that RS is caused by the early separation of the 'thickened' turbulent boundary layer on the seam side compared to the separation of the 'thinner' turbulent boundary layer on the non-seam side (described in more detail in § 1). According to this hypothesis, $\overline{C}_D$ should increase with increase in Re as the flow transitions from CS to RS state (Achenbach 1972). However, figure 6 shows that this transition is accompanied by a decrease in $\overline{C}_D$. This observation motivates us to further investigate the phenomena of CS and the transition to RS. We also explore the role of seam *vis-à-vis* formation of an LSB in the transition.

3.3. *Modelling a new cricket ball as a sphere with trip(s)*

Figure 7 depicts the variation of $\overline{C}_D$ and $\overline{C}_Z$ with Re for a sphere with five trips, a sphere with one trip and a new cricket ball (reproduced from figure 6). The trip/seam angle in all these cases is $\phi_T = 30°$. For the case of the sphere with one trip, force measurements were conducted on both the models – with and without pressure ports.

The value of $\overline{C}_Z$ on the sphere with five trips is close to zero (NS) for $Re < 0.5 \times 10^5$ approximately. This may be attributed to the laminar boundary layer separation from the surface of the ball being almost axisymmetric (Mehta *et al.* 1983; Scobie *et al.* 2012). The increase of $\overline{C}_Z$ beyond this Re marks the onset of the regime of CS.

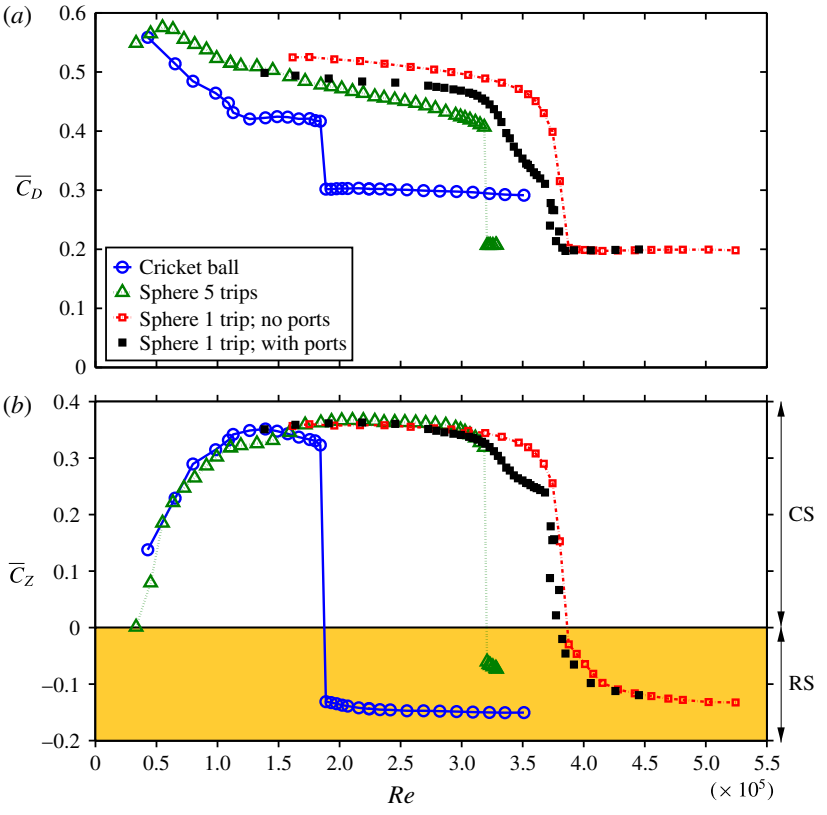

FIGURE 7. (Colour online) Variation of (*a*) $\overline{C}_D$ and (*b*) $\overline{C}_Z$ with Re for a cricket ball, a sphere with five trips and a sphere with one trip. In all cases the trip/seam angle with the free stream is $\phi_T = 30°$. Positive values of $\overline{C}_Z$ correspond to CS, while negative values lead to RS. The same is marked in (*b*) and highlighted via background colour.

The NS regime is completely missed out for the sphere with one trip since the flow is already in the CS regime for the lowest Re tested. With further increase in Re, there is an abrupt switch in the direction of the lateral force, accompanied by a steep fall in $\overline{C}_D$. This marks the onset of the RS regime, which occurs at different Re for the various models. An interesting observation from figure 7 is that the peak value of $\overline{C}_Z$ is independent of the model. For all the models, it is approximately 0.35 and -0.15 for the CS and RS regimes, respectively. Further, the magnitude of the maximum lateral force coefficient in the RS regime ($\approx$0.15) is significantly lower than that in the CS regime ($\approx$0.35).

It is further observed from figure 7 that the variation of force coefficients with Re is qualitatively similar for all models. However, the critical Re for transition from CS to RS is different for the various models. Specifically, the transition occurs at a significantly lower Re for a new cricket ball as compared to that for a sphere with trip(s). This suggests that the inherent surface roughness of a new cricket ball, and its distribution, has a prominent influence on the transition. It also implies that the quality of the leather, embossing of the logo of the manufacturer, and the variations in the manufacturing process amongst various brands may significantly affect the

critical Re for the transition. In fact, since the manufacturing process renders certain differences from one sample to another even when the specimens are from the same brand/manufacturer, one can expect ball-to-ball variations in the magnitude of the coefficient of swing force at a specific Re, and the critical Re corresponding to the reversal in the swing force. Therefore, to eliminate the uncertainties associated with the geometric irregularities and surface roughness in a real cricket ball, all the studies related to flow diagnostics are reported for a sphere with trip(s). We note, however, that, since the inherent surface roughness associated with a new ball has a relatively strong influence on the transition of the flow (figure 7), the flow phenomena that cause transition for the new ball and the sphere with trip(s) might not be exactly the same. Nevertheless, the qualitative similarity in the variation of the force coefficients with Re for various models motivates us to model the new cricket ball via a sphere with trip(s).

3.4. *Surface oil-flow visualization*

An oil-flow study was conducted on the sphere with one trip and five trips to understand the flow structures in various flow regimes. The model with five trips enters the RS regime for free-stream speed of the flow in the tunnel beyond 70 m s^{-1} (figure 7). We were unable to conduct oil-flow visualization at such large speeds. The visualizations for this model in NS and CS regimes are shown in figure 8. A schematic of the observed flow is also shown at each Re.

Figure 8(a) shows the flow in the NS regime. Despite the seam being oriented at an angle to the free stream, the flow is fairly axisymmetric and similar to the subcritical flow past a smooth sphere (figure 5b). The laminar boundary layer separates at $\phi \approx 80^\circ$ from the seam side as well as the non-seam side of the sphere. With an increase in Re, the flow enters the CS regime (figure 7). Figure 8(b) shows the flow in the initial stages of the CS regime. This regime is characterized by the boundary layer transition on the seam side, resulting in the formation of an LSB and delay of eventual flow separation. The flow on the non-seam side, however, is devoid of an LSB and similar to that in the NS regime. The region of formation of an LSB on the seam side, in terms of the polar angle, is $-60^\circ < \theta < 60^\circ$. In this region, the laminar boundary layer separates at $\phi \approx 100^\circ$ and undergoes a turbulent reattachment at $\phi \approx 115^\circ$. The turbulent boundary layer separates further downstream at $\phi \approx 135^\circ$. On the other hand, in the region where the seam is closer to the shoulder ($60^\circ < \theta < 80^\circ$ and $-80^\circ < \theta < -60^\circ$), the boundary layer directly trips to a turbulent state on encountering the seam (Son *et al.* 2011). Hence, no LSB is observed in this region. The presence of residual oil in the regions $80^\circ < \theta < 90^\circ$ and $-90^\circ < \theta < -80^\circ$ suggests that the flow separates directly after encountering the trip/seam and does not reattach (Igarashi 1986). The extent of the LSB decreases in both the azimuthal and polar directions with increase in Re. At the same time, the region where the flow directly transitions to a turbulent state due to the trip/seam increases with increase in Re. For example, in figure 8(c,d), the extent of the LSB is reduced to approximately $-30^\circ < \theta < 30^\circ$ and $-15^\circ < \theta < 15^\circ$, respectively. At $Re = 2.82 \times 10^5$ (figure 8e), the boundary layer on the bulk of the seam side of the sphere achieves a turbulent state right after the seam and the LSB completely disappears from this side of the sphere.

Figure 9 shows pictures from the oil-flow study at various Re in the CS and RS regimes for the sphere with one trip. The observations in the CS regime (figure 9a,b) are consistent with those from the sphere with five trips (figure 8). In the RS regime (figure 9c), the boundary layer transitions on the non-seam side of the sphere, resulting

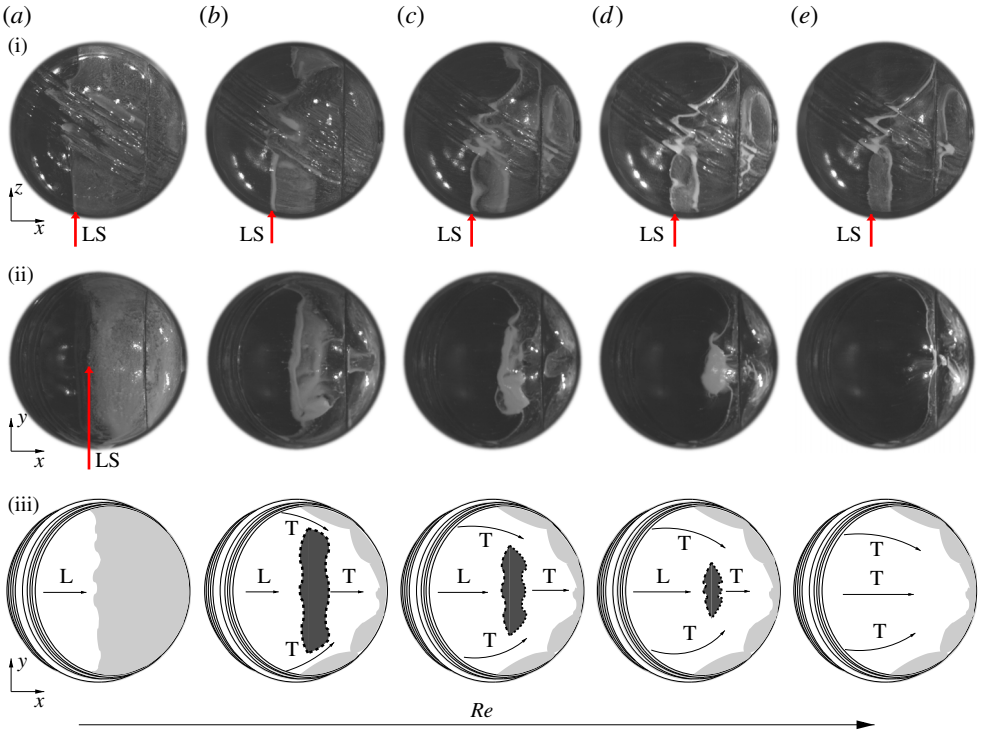

FIGURE 8. (Colour online) Oil-flow patterns on a sphere with five trips at $\phi_T = 30°$ at various Re: (*a*) $Re = 0.44 \times 10^5$ (NS), (*b*) $Re = 1.11 \times 10^5$ (CS), (*c*) $Re = 1.72 \times 10^5$ (CS), (*d*) $Re = 2.22 \times 10^5$ (CS) and (*e*) $Re = 2.82 \times 10^5$ (CS). The images in row (i) have been taken by a camera placed outside the roof of the tunnel, while those in row (ii) show the flow on the seam side taken by a camera placed outside the sidewall of the tunnel. A schematic of the flow on the seam side is shown in row (iii). The vertical lines with arrows indicate the approximate azimuthal locations of laminar boundary layer separation (LS) from the sphere. In (iii), L and T represent a laminar and turbulent boundary layer, respectively. The approximate region occupied by the LSB is shown via dark shading, bounded by broken lines. The region of flow separation beyond which there is no further reattachment is marked by lighter shading.

in an LSB on this side. The LSB on the non-seam side is similar to that observed for the supercritical flow over a smooth sphere (figure 5*c*). The laminar boundary layer separates at $\phi \approx 105°$, undergoes a turbulent reattachment at $\phi \approx 120°$ and eventually separates at $\phi \approx 135°$. On the other hand, the azimuthal location of the separation point of the turbulent boundary layer on the seam side moves upstream as the flow transitions from the CS to RS regime: from $\phi \approx 135°$ in CS (figure 9*b*) to $\phi \approx 125°$ in the RS regime (figure 9*c*). Further, at this Re, the LSB on the seam side is restricted to a very small region near $\theta = 0°$. It disappears completely at a larger Re (not shown here), similar to our observation for a sphere with five trips (figure 8*e*). In general, the size of the LSB, on the seam side, decreases with increase in Re.

3.5. *Flow physics associated with the swing of a new cricket ball: a hypothesis*

Utilizing the oil-flow visualizations and force measurements from the present study as well as results from our earlier study on a smooth sphere (Deshpande *et al.* 2017), we

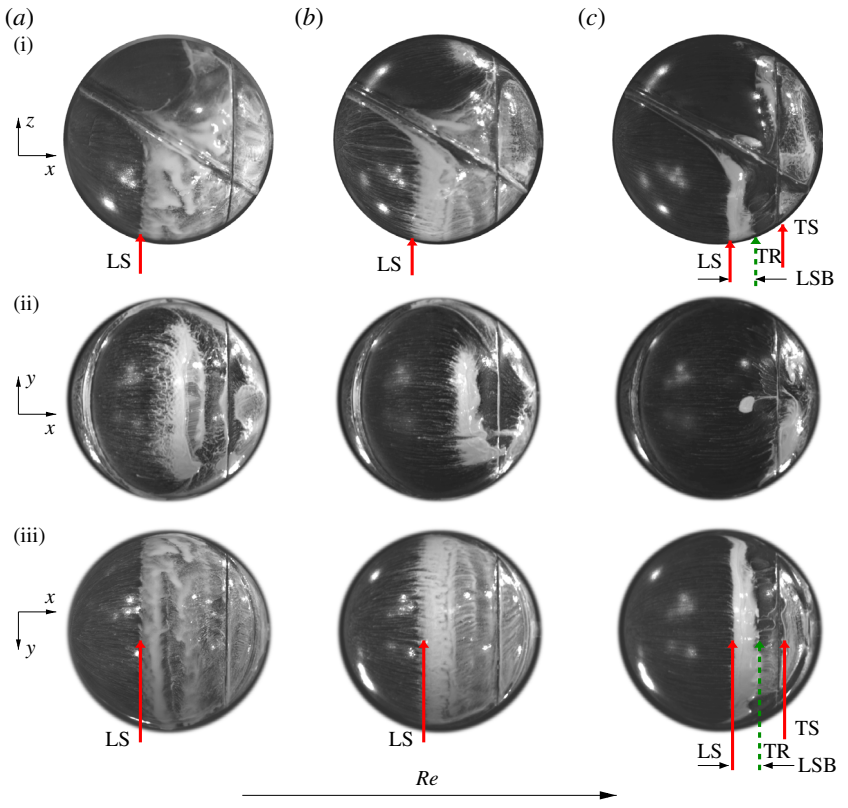

FIGURE 9. (Colour online) Oil-flow patterns on a sphere with one trip at $\phi_T = 30°$ at various Re: (*a*) $Re = 1.72 \times 10^5$ (CS), (*b*) $Re = 2.82 \times 10^5$ (CS) and (*c*) $Re = 3.92 \times 10^5$ (RS). The images in row (i) show the top view while those in rows (ii) and (iii) show the seam and non-seam sides, respectively. The separations of the laminar and turbulent boundary layers are marked in the images as LS and TS, respectively. TR corresponds to the reattachment of the turbulent boundary layer.

propose the possible aerodynamic phenomena that lead to the swing force experienced by the new cricket ball. To this extent, a schematic of the flow in various regimes is shown in figure 10 along with the variation of the aerodynamic force coefficients with Re. At relatively low Re, the seam does not play a significant role. The boundary layer is laminar on the entire surface and separates nearly axisymmetrically (figure 10*a*) just upstream of the shoulder. Consequently, $\overline{C}_Z$ is close to zero and we refer to this regime as the NS regime. The $\overline{C}_D$ is relatively large (figure 10*d*) owing to a wide wake.

Beyond a certain Re, the flow becomes unstable to the disturbance introduced by the seam. This causes a transition of the boundary layer on the seam side of the model. The onset of the transition is marked by the intermittent formation of an LSB (Deshpande *et al.* 2017) on the major part of the seam side of the sphere/ball. The flow on the non-seam side remains laminar. This flow asymmetry leads to a lateral force on the model in the direction of the seam. This is the regime of CS. The delay in flow separation on the seam side leads to a reduction in the drag coefficient. The fraction of time for which the LSB exists increases with increase in Re. Thus, $\overline{C}_D$ decreases while $\overline{C}_Z$ increases with increase in Re. Beyond a certain

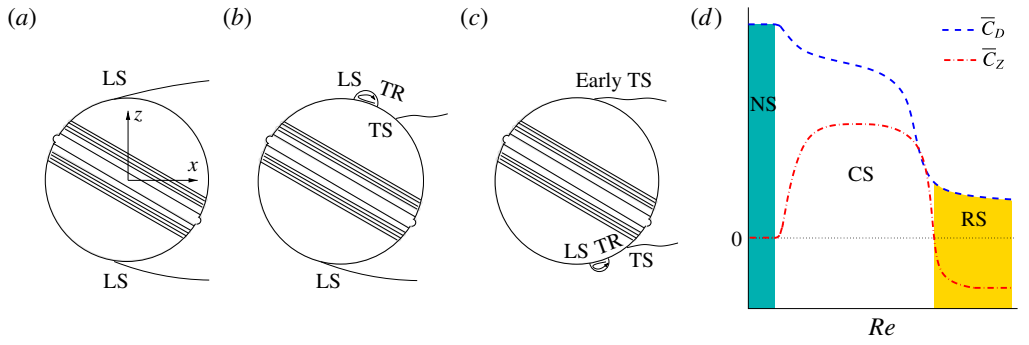

FIGURE 10. (Colour online) Hypothesis of the flow past a new cricket ball. Schematic of the flow in various regimes: (*a*) NS, (*b*) CS and (*c*) RS. The acronyms LS, TR and TS represent laminar separation, turbulent reattachment and turbulent separation, respectively. (*d*) Variation of $\overline{C}_D$ and $\overline{C}_Z$ with *Re*. The various flow regimes are also marked in the plot.

Re, the LSB is no longer intermittent and exists at all times. The $\overline{C}_Z$ value saturates to approximately 0.35. The size of the LSB reduces with further increase in *Re*. It completely disappears beyond a certain *Re*. In this state, the flow on the major part of the seam side achieves a turbulent state just downstream of the seam.

At a certain *Re*, the boundary layer on the non-seam side undergoes transition via formation of an LSB. This leads to a downstream shift in the flow separation causing an increased suction on this side of the model. As a result, there is a reversal in the direction of the lateral force on the model; it is now away from the seam. This is the regime of RS. This phenomenon is accompanied with an upstream shift of the flow separation on the seam side along with a reduction in the peak suction on that side of the model. The LSB is intermittent at the onset of the RS regime. In this situation $\overline{C}_Z$ and $\overline{C}_D$ decrease with increase in *Re*. They remain constant with increase in *Re* once the LSB is fully developed and no longer intermittent. At a sufficiently large *Re*, the flows on both the seam and non-seam sides achieve a similar state. The flow regains an almost symmetric state corresponding to the NS regime. We carry out pressure measurements to further test the hypothesis. We note that the proposed hypothesis on the possible flow structures for flow past the ball, during NS, CS and RS, is based on the observations for flow past an idealized cricket ball, i.e. a smooth sphere with trip(s). In that sense, it does not account for the influence that the inherent surface roughness of a new cricket ball might have on the flow mechanisms (refer to § 3.3).

An interesting phenomenon during CS is that, even though the transition of the boundary layer occurs on the seam side, the effect is felt by the non-seam side as well in terms of an upstream shift of the separation point. We recall that the Kutta–Joukowski theorem relates the lift generated by a body, such as an airfoil or spinning cylinder, to the circulation around it (Anderson 1991). We note that the lateral force generated by the ball during CS can be modelled via a circulation of appropriate magnitude (in the clockwise direction about the *y*-axis of the ball as per figure 10*b*). This circulation affects the pressure distribution as well as the flow separation on both sides of the ball. Similarly, an anticlockwise circulation in the regime of RS slows the flow near the shoulder on the seam side. This leads to relatively lower suction and upstream shift of the flow separation point on the seam side of the ball.

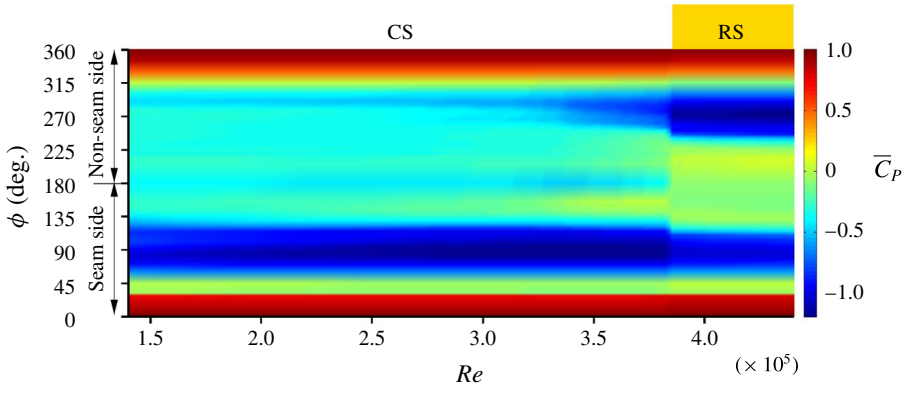

FIGURE 11. (Colour online) Flow past a sphere with one trip at $\phi_T = 30°$: variation of mean coefficient of pressure on the ϕ–Re plane. The data presented here have been acquired from the pressure ports lying on the circumferential line C (shown in figure 4).

3.6. *Surface-pressure measurements*

Figure 11 shows the angular distribution of time-averaged pressure coefficient ($\overline{C}_P$) with Re for the sphere with one trip, along the circumferential line C (figure 4). The asymmetry in the surface-pressure distribution between the seam and non-seam sides, in the CS and RS flow regimes, is clearly visible. The changes in $\overline{C}_P$ from the CS to RS regime occur over a relatively narrow range of Re. This is consistent with the variation of coefficient of forces acting on the ball with Re (figure 7). To highlight some of the salient features of the flow, the line plots of $\overline{C}_P$ with ϕ are shown in figure 12(*a*) at certain Re. An interesting observation from figure 12(*a*) is the resemblance in the pressure distribution on the non-seam side with that on the smooth sphere (from Deshpande *et al.* 2017), for a comparable Re.

The $\overline{C}_P$ distribution for $Re = 1.64 \times 10^5$, in figure 12(*a*), shows a plateau on the seam side for $100° \leqslant \phi \leqslant 115°$. This signifies the presence of an LSB in this region (Deshpande *et al.* 2017). To understand the structure of the LSB at other non-zero polar locations on the surface of the model, the $\overline{C}_P$ distribution at ports located along circumferential lines A, B, D and E (figure 4 and table 2) is shown in figure 12(*b*).

The symmetry of the model about line C is utilized to plot data for ports on lines A ($\theta = 60°$) and E ($\theta = -60°$) together and referred to as data along line A–E. The case with line B–D is similar. The size of the LSB decreases in both polar and azimuthal directions with increase in Re, which is consistent with the observations from the oil-flow study. The decrease in the azimuthal direction is mostly due to the downstream shift of the location of laminar boundary layer separation, while the turbulent reattachment remains fixed at $\phi \approx 115°$. In terms of the variation in the polar direction, the LSB disappears from the seam side along line B–D at $Re \approx 3.26 \times 10^5$ and then along C at a slightly higher $Re \approx 3.83 \times 10^5$.

For all Re corresponding to the CS regime, the turbulent boundary layer separates at $\phi \approx 135°$ on the seam side. This is inferred from the constant pressure distribution on the leeward side of the sphere. The onset of the transition of the boundary layer on the non-seam side of the model marks the beginning of the RS regime. Figure 12(*a*) shows the presence of an LSB on the non-seam side for $Re = 4.23 \times 10^5$ and 4.43×10^5. The reattached boundary layer eventually separates at $\phi \approx 225°$, leading to a significant increase in suction over the non-seam side. The azimuthal location of the

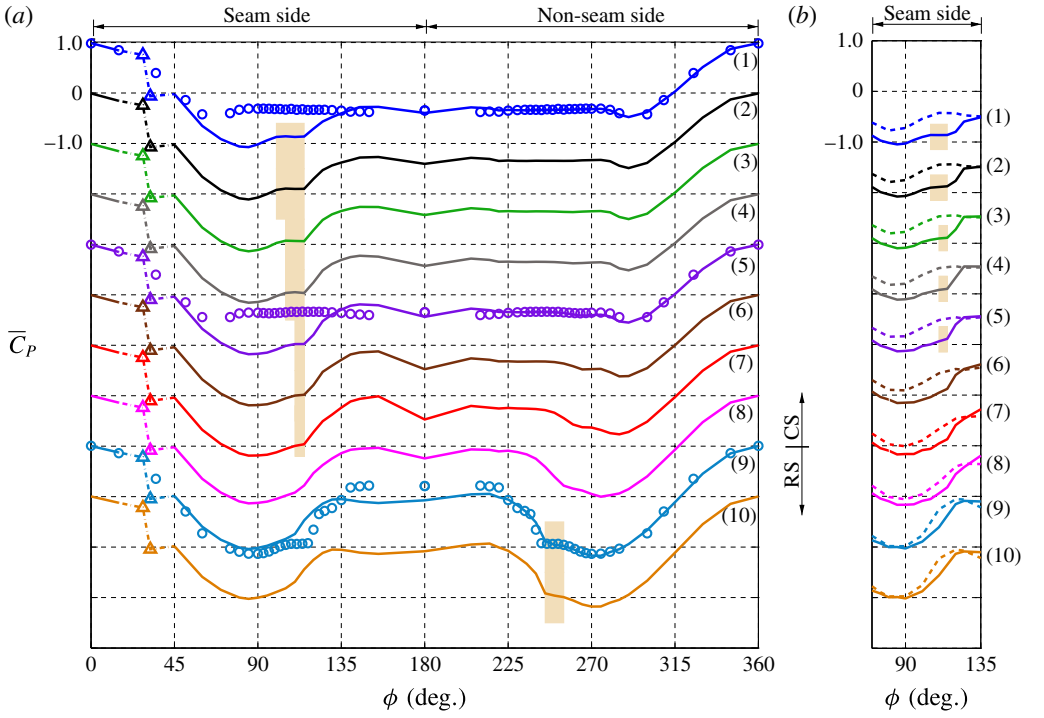

FIGURE 12. (Colour online) Angular distribution of time-averaged pressure coefficient ($\overline{C}_P$) on a sphere with one trip at $\phi_T = 30°$ (lines) and a smooth sphere (○) at various *Re*: (1) 1.64×10^5, (2) 1.91×10^5, (3) 2.18×10^5, (4) 2.45×10^5, (5) 2.86×10^5, (6) 3.26×10^5, (7) 3.52×10^5, (8) 3.83×10^5, (9) 4.23×10^5 and (10) 4.43×10^5. The data for a sphere with one trip in (*a*) have been acquired from the pressure ports lying on the circumferential line C, while data in (*b*) have been acquired from the ports lying on the lines A–E (dashed) and B–D (solid), respectively. The shaded region indicates the approximate angular location where an LSB is observed. Triangles joined by broken lines indicate $\overline{C}_P$ values measured at the pressure ports just upstream and downstream of the trip.

separation point on the seam side changes, from $\phi \approx 135°$ (CS) to $\phi \approx 125°$ (RS) (figures 11 and 12), during the switch from CS to RS. It leads to loss in peak suction on the seam side of the model and further adds to the magnitude of the swing force towards the non-seam side.

The variation of the relative suction, between the seam and non-seam sides, with *Re* is particularly interesting (figures 11 and 12*a*). It undergoes a sharp change during the CS–RS transition. We define the difference between the $\overline{C}_P$ distribution on the two sides as: $\Delta\overline{C}_P(\phi) = [(\overline{C}_P)_s(\phi) - (\overline{C}_P)_{ns}(\phi)]$. Its variation along line C, for various *Re*, is shown in figure 13 and is useful in understanding the lateral force experienced by the model. We note that a negative value of $\Delta\overline{C}_P(\phi)$ implies a higher suction on the seam side (i.e. a positive C_Z). Similarly, a positive value corresponds to a larger relative suction on the non-seam side (i.e. a negative C_Z).

The $\Delta\overline{C}_P$–ϕ distribution is virtually identical for all the *Re* in the regime of RS. In the regime of CS, it is again insensitive to *Re*, except in the region downstream of the shoulder, where the change is associated with the activity related to the LSB (figure 12). As the *Re* increases in the CS regime, the decrease in $\Delta\overline{C}_P$ in the range

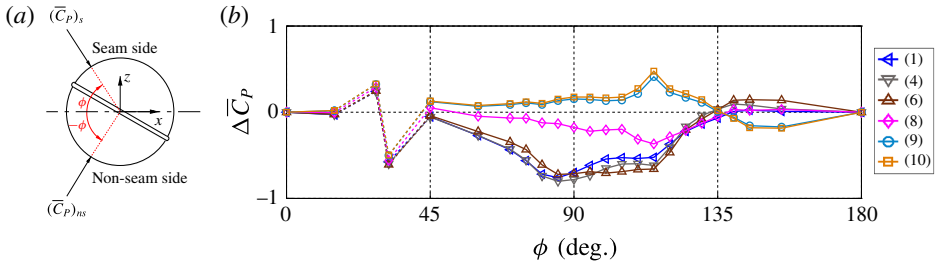

FIGURE 13. (Colour online) (*a*) A schematic for defining $\Delta\overline{C}_P$. (*b*) Angular distribution of $\Delta\overline{C}_P$ along the circumferential line C of the sphere with one trip at various *Re*: (1) 1.64×10^5, (4) 2.45×10^5, (6) 3.26×10^5, (8) 3.83×10^5, (9) 4.23×10^5 and (10) 4.43×10^5. The plots follow the same legend as used in figure 12. Symbols joined by broken lines indicate $\overline{C}_P$ values measured at the pressure ports just upstream and downstream of the trip.

$90° < \phi < 120°$ is accompanied by its increase in $135° < \phi < 155°$. Therefore, in both the CS and RS regimes the lateral force coefficient is largely constant with *Re* (figure 7). It is also observed that the net differential suction is larger in the CS regime as compared to that in the RS regime. This is consistent with the force experienced by the model in the CS ($\overline{C}_Z \sim 0.35$) and RS ($\overline{C}_Z \sim -0.15$) regimes. An interesting observation from figure 13(*b*) is that the peak of the relative suction in the CS regime is just upstream of the shoulder while it is at $\phi \approx 120°$ in the RS regime (figure 13*a*). In the CS regime, the primary contribution to $\Delta\overline{C}_P$ is from the high relative suction in the shoulder region on the seam side. On the other hand, in the RS regime, the main difference is the presence of a prominent LSB on the non-seam side as opposed to its absence/reduced size on the seam side.

3.7. *Switch between the flow regimes: intermittency of the LSB*

The switch between the flow regimes, for example CS to RS, is explored. Figures 6, 7 and 11 suggest that the transition from CS to RS is caused by the formation of an LSB on the non-seam side. This observation raises a question: Does the LSB, on the model sphere with a trip, involve intermittency (Deshpande *et al.* 2017) during the early stages of transition? The middle row of figure 14 shows the time variation of C_D and C_Z for the model with one trip at $Re = 3.83 \times 10^5$. This *Re* lies in the very narrow band of *Re* where the flow transitions from the CS to RS regime (figures 7 and 12). The time histories of both C_D and C_Z show an intermittent transition between bistable states: a positive C_Z (CS) and negative C_Z (RS). Also shown for reference are the time histories of C_D and C_Z for $Re = 3.68 \times 10^5$ and 3.92×10^5 corresponding to CS and RS states, respectively.

Figure 15(*a*) shows the space–time diagram of the C_P distribution on the circumferential line C for $Re = 3.83 \times 10^5$. The C_P distribution also exhibits a switch between bistable states. The CS and RS states are identified in figure 15(*a*) via the relative strength of the suction on two points on the shoulder corresponding to $\phi = 90°$ (seam side) and 270° (non-seam side). Conditional averaging of the C_P distribution is carried out for the CS and RS states. These values are referred to as $\langle C_P \rangle_{CS}$ and $\langle C_P \rangle_{RS}$, respectively. Figure 15(*b*) shows these conditionally averaged distributions as well as the time-averaged distribution for the entire duration of measurement ($\overline{C}_P$). A plateau is observed in the $\langle C_P \rangle_{RS}$ distribution for approximately

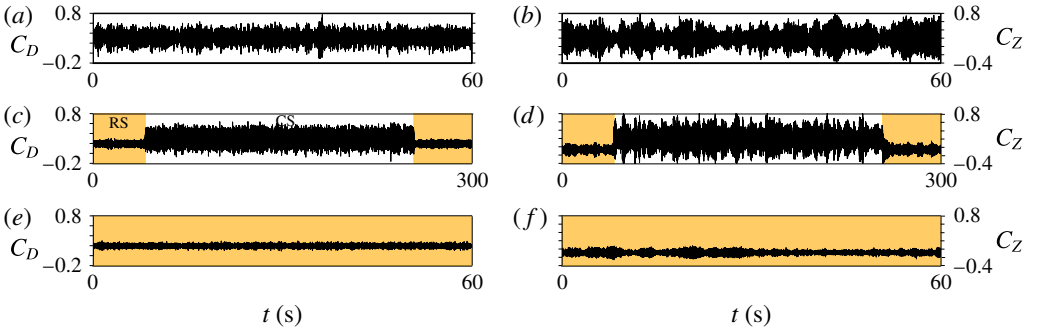

FIGURE 14. (Colour online) Time histories of C_D (a,c,e) and C_Z (b,d,f) for flow past a sphere with one trip at $\phi_T = 30°$ at $Re = 3.68 \times 10^5$ (a,b), 3.83×10^5 (c,d) and 3.92×10^5 (e,f). The CS and RS flow regimes are indicated by white and off-white background colours, respectively.

$240° \leqslant \phi \leqslant 255°$. This suggests the presence of an LSB on the non-seam side for the time duration when the flow is in the state of RS. Such a plateau is not observed in the distribution for $\langle C_P \rangle_{CS}$ or that for $\overline{C}_P$, reaffirming that the CS–RS transition is a consequence of the formation of an LSB on the non-seam side. We also note that none of the three distributions suggest an LSB on the seam side, which is consistent with figures 9 and 12. Figure 15 brings out the difference in the azimuthal location of the final separation point between the CS and RS states. It shows that the turbulent flow separation point on the seam side moves upstream as the flow switches from CS to RS.

Intermittency of the LSB is also observed at the onset of transition of the CS regime. A detailed analysis was carried out for the instantaneous force coefficients recorded for the model sphere with five trips at $Re = 0.6 \times 10^5$ (not shown here). The analysis confirmed the intermittent nature of the LSB on the seam side. In this case, C_Z exhibits alternate switching between two mean states: (i) a state devoid of an LSB and with zero lateral force ($\langle C_Z \rangle_{NS} = 0$), and (ii) a state with an LSB on the seam side and positive lateral force ($\langle C_Z \rangle_{CS} \approx 0.24$).

3.8. *Flow past a rough cricket ball*

The effect of roughness on the force on a cricket ball is studied for $\phi_T = 30°$. Figure 16 shows the variation of $\overline{C}_D$ and $\overline{C}_Z$ with Re for a new ball, a ball with seam side rough (S–R), a ball with non-seam side rough (NS–R) and a completely rough ball (C–R). Figure 16 also shows the schematic of the various cases. Although a different specimen of the SG Test cricket ball was used for this set of experiments, the variation of the force coefficients for the new ball (figure 16) is in reasonable agreement with those shown in figure 6. Compared to a new ball, the model S–R begins to swing (CS) at a lower Re. The peak $\overline{C}_Z$ for CS is approximately 0.25 and is lower than that for a new ball (∼0.35). As suggested by Achenbach (1974) for a rough sphere, perhaps an LSB does not form on the roughened seam side, leading to an upstream location of the transition of the boundary layer compared to that on the new ball. This leads to reduced asymmetry in the pressure distribution on the two halves and, therefore, a lower peak force coefficient for CS. The switch from CS to RS is abrupt and occurs at an Re similar to that for a new ball. The peak magnitude

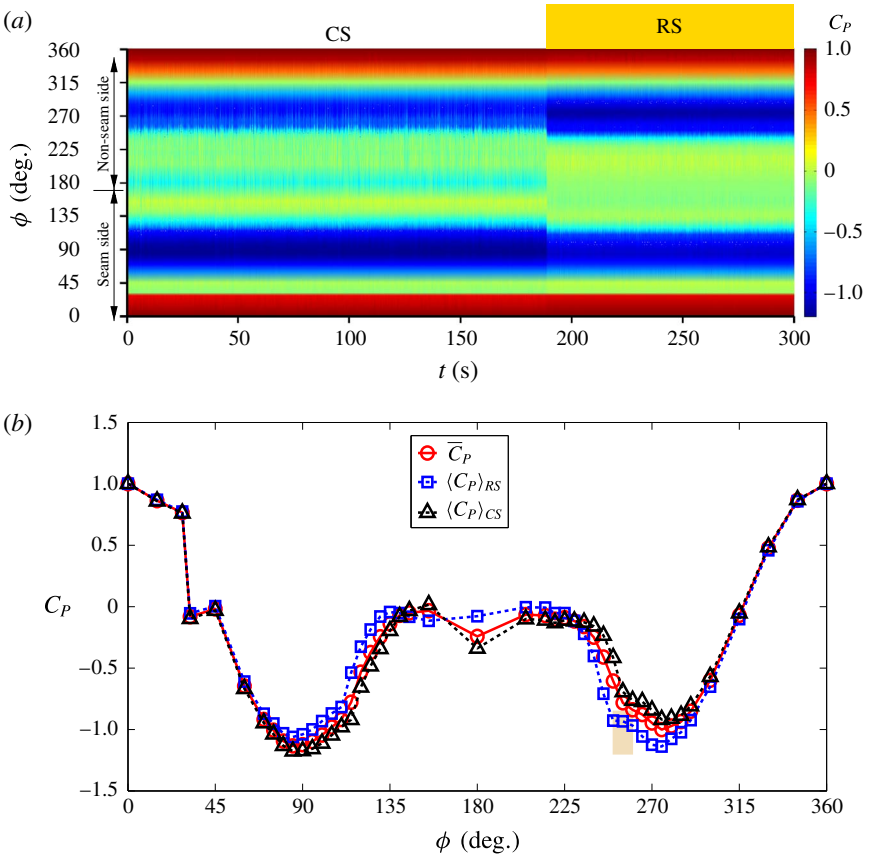

FIGURE 15. (Colour online) Distribution of the coefficient of pressure (C_P) on the surface of the sphere with one trip at $Re = 3.83 \times 10^5$ and $\phi_T = 30°$ for the pressure ports lying on the circumferential line C. (*a*) Space–time diagram of C_P. Also marked are the regimes corresponding to CS and RS. (*b*) Angular distribution of the conditional time-averaged pressure coefficient for states CS ($\langle C_P \rangle_{CS}$, triangles) and RS ($\langle C_P \rangle_{RS}$, squares). Also shown is the time-averaged C_P ($\overline{C}_P$, circles). The approximate angular location where an LSB is observed in the flow state corresponding to RS is indicated via shading.

for RS, however, is significantly larger (∼0.22) as compared to the new ball (∼0.15). This is because the turbulent boundary layer on the roughened seam side separates at a relatively upstream location compared to that for a new ball. This creates larger asymmetry in the pressure for the S–R model in the RS regime. It also leads to a wider wake and, therefore, a larger $\overline{C}_D$.

The flow past model NS–R is very interesting; the roughness on the non-seam side appears to be more effective than the seam (on the seam side) in causing the transition of the boundary layer. Therefore, unlike a new ball, the transition of the boundary layer occurs first on the non-seam side. As a result, the NS–R model undergoes a switch from NS to RS directly, and at a fairly low Re (figure 16). The transition on the seam side is similar to that for a new ball. The $\overline{C}_D$ value decreases with increase in Re up to $Re \sim 1.0 \times 10^5$. This marks the completion of transition of the boundary layer on both halves of the ball. As suggested by Achenbach (1974) for a rough sphere, further increase in Re causes gradual upstream movement of the transition and

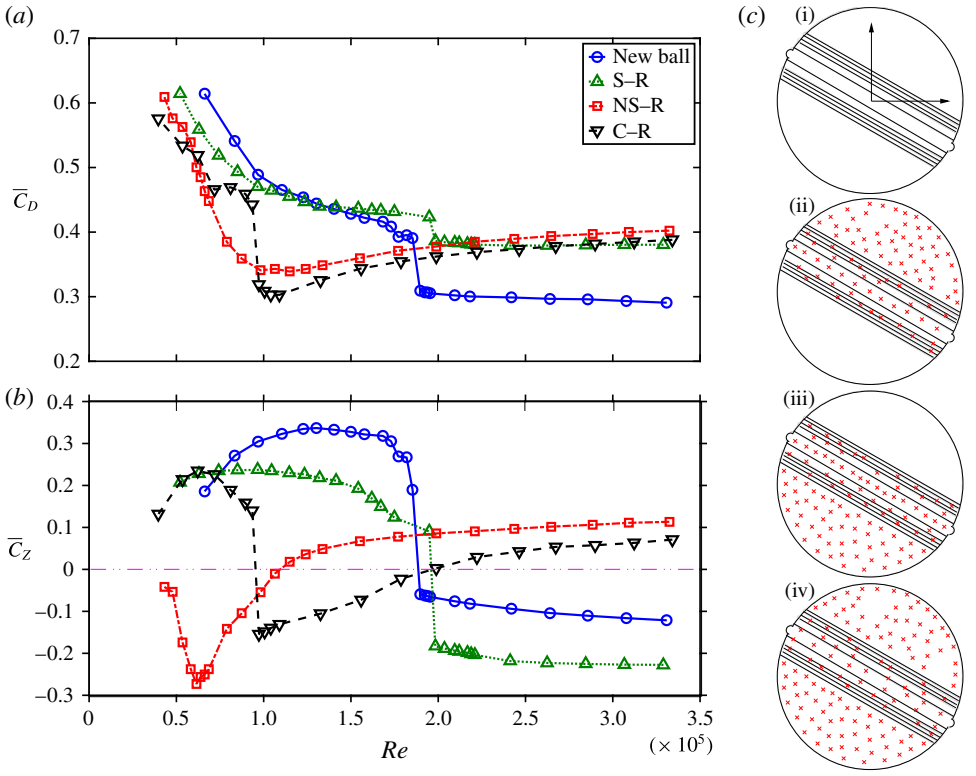

FIGURE 16. (Colour online) Variation of (*a*) $\overline{C}_D$ and (*b*) $\overline{C}_Z$ with Re for a new and a roughened cricket ball. In all cases the trip/seam angle with the free stream is $\phi_T = 30°$. Positive values of $\overline{C}_Z$ correspond to CS, while negative values lead to RS. (*c*) Schematic of the various states of the cricket ball: (i) new ball, (ii) roughened seam side (case S–R), (iii) roughened non-seam side (case NS–R) and (iv) completely roughened cricket ball (case C–R). The seam is also roughened in cases S–R and NS–R.

separation points on the roughened non-seam side of the ball. This results in a very gradual increase in $\overline{C}_D$ as well as $\overline{C}_Z$ with increase in Re.

The sequence of onset of CS and RS for the completely roughened (C–R) model is the same as that for a new ball, but each event occurs at a significantly lower Re. This is consistent with our earlier observation related to figure 7 wherein the CS–RS transition for a new ball, owing to its inherent surface roughness, occurs at a relatively lower Re compared to a sphere with trip(s). The value of $\overline{C}_D$ decreases and $\overline{C}_Z$ increases with increasing Re for $Re < 0.7 \times 10^5$ (figure 16), suggesting that the transition on the seam side of the ball leads to CS. As expected, the peak $\overline{C}_Z$ is the same as that for model S–R; it is lower than that for a new ball. The change from CS to RS is due to the transition of the boundary layer on the non-seam side. It is abrupt (at $Re \sim 1.0 \times 10^5$) and is accompanied by a significant fall in $\overline{C}_D$. Both $\overline{C}_D$ and $\overline{C}_Z$ are close to their minimum values at this Re, signifying a complete transition of the boundary layer on the non-seam side. The peak magnitude of $\overline{C}_Z$ for RS for this case is smaller than that for the model NS–R. This is due to laminar separation, at the corresponding Re, for model NS–R, and a turbulent separation for the model C–R, on the seam side of the respective models. Further increase in Re leads to upstream

movement of the transition and separation points on the non-seam side of the model C–R leading to increase in $\overline{C}_D$ and $\overline{C}_Z$. The azimuthal location of the separation point of the flow on the seam and non-seam sides is nearly the same at $Re \sim 2.0 \times 10^5$, leading to $\overline{C}_Z \sim 0$. The model undergoes CS, albeit of low magnitude, with further increase in Re.

3.9. *Trajectory of a cricket ball*

We estimate the trajectory of a new as well as rough balls, delivered at a certain initial speed and seam orientation, by integrating the following equation in time: $m(\mathrm{d}\boldsymbol{V}/\mathrm{d}t) = \boldsymbol{F}$. Here, m is the mass of the cricket ball, $\boldsymbol{V}$ its velocity and $\boldsymbol{F}$ the force acting on it. We restrict our attention to the motion of the ball in a horizontal plane and assume that the ball maintains its initial seam position throughout its trajectory and is devoid of any spin. We note that $\overline{C}_Y \approx 0$ for a non-spinning ball. In reality, a swing bowler would typically impart back-spin on the ball, leading to non-zero $\overline{C}_Y$. In this work, we do not consider the motion of the ball in the vertical plane. The interested reader may refer to the work by Baker (2010), which presents the vertical trajectory of the ball solely due to the action of gravity. The lateral component of velocity of the ball at the time of delivery is assumed to be zero. It is further assumed that the aerodynamic force acting on the ball at each time instant is the time-averaged force on the ball for the fully developed flow at the corresponding value of instantaneous Re. The force measurements from the wind-tunnel testing of the SG Test cricket ball are utilized to estimate $\boldsymbol{F}$. Assuming that the ambient conditions correspond to normal temperature and pressure (20 °C, 1 atm), the variation of lateral force and drag with speed, for a new and roughened SG Test cricket ball of diameter 71 mm, are shown in figures 17 and 18. Force $\boldsymbol{F}$ at each time instant is estimated by interpolating the data for the corresponding Re from these figures. The mass of the ball is assumed to be the same as that of the standard SG Test cricket ball (= 0.156 kg). A time step of 0.001 s is utilized to integrate the equation of motion.

3.9.1. *New cricket ball*

We observe from figure 17 that the variation of the drag and lateral force with speed is qualitatively similar for all ϕ_T. Its main effect is the speed at which NS switches to CS, and CS to RS. Of the three seam orientations considered, the CS–RS change-over occurs at the lowest speed for $\phi_T = 20°$. It has been shown by Mehta (1985) that $\phi_T = 20°$ is the optimum angle for swing bowling. Figure 19 shows the streamwise speed of the ball and its lateral movement as it travels down the pitch of length 22 yards (≈20.12 m), for $\phi_T = 20°$ and various initial speeds. The streamwise speed of the ball, during its travel to the end of the pitch, decreases by 11.9 % when its initial speed is 90 km h^{-1} and by 9.2 % when the initial speed is 165 km h^{-1}. This is consistent with the results of Baker (2010), who reported a decrease of 8–13 % for initial speeds lying between 90 and 153 km h^{-1}. The initial speed of the ball has a very significant effect on its trajectory. The ball experiences CS at relatively low initial speeds and RS at higher speeds. The trajectories of the balls delivered at speeds corresponding to the CS regime are similar to those reported by Mehta (2005). Also shown are the measurements by Imbrosciano (1981) for a cricket ball delivered at an approximate initial speed of 108 km h^{-1}. The streamwise variation of the lateral movement of the ball is in reasonable agreement with the present estimates.

To bring out the very significant role of the orientation of the seam, and the various types of possible trajectories, figure 20 shows the lateral deflection of the ball

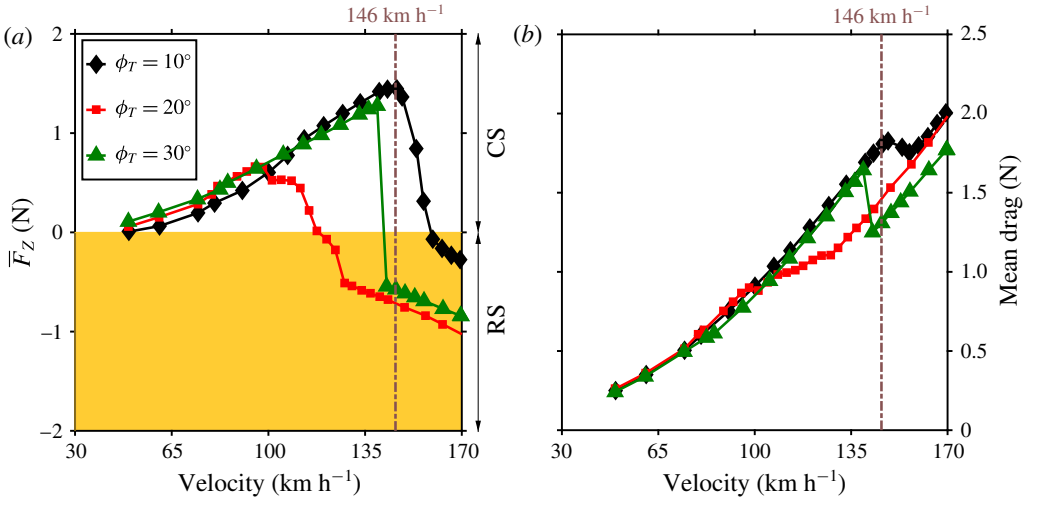

FIGURE 17. (Colour online) Variation of time-averaged (*a*) swing force ($\overline{F}_Z$) and (*b*) drag force ($\overline{F}_D$) with speed (km h^{-1}) measured for a new cricket ball oriented at various seam angles ϕ_T.

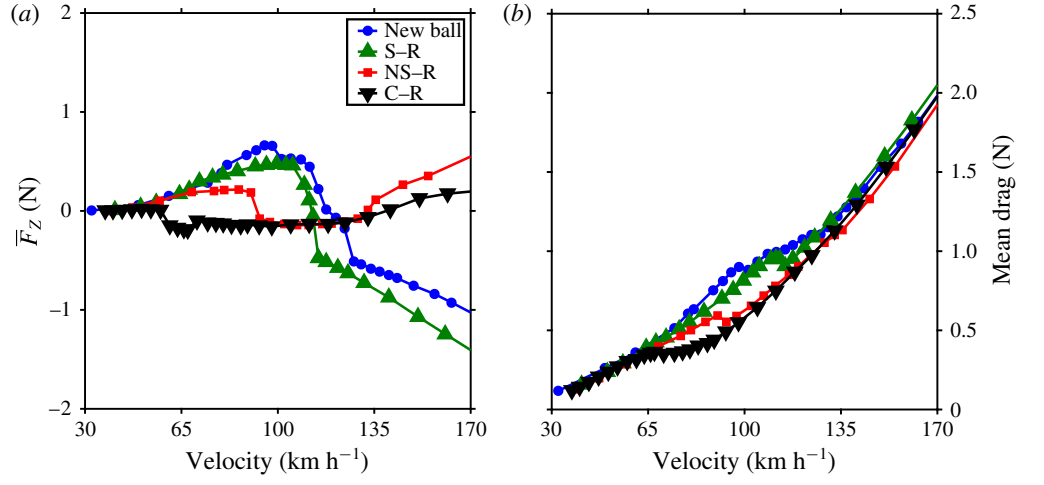

FIGURE 18. (Colour online) Variation of time-averaged (*a*) swing force ($\overline{F}_Z$) and (*b*) drag force ($\overline{F}_D$) with speed (km h^{-1}) measured for a new as well as roughened cricket balls oriented at a seam angle $\phi_T = 20°$.

delivered at 146 km h^{-1}, for three values of ϕ_T. The ball with $\phi_T = 10°$ undergoes CS while the one with $\phi_T = 20°$ exhibits RS. The case of $\phi_T = 30°$ is very interesting. At this speed, on its release, the ball experiences a lateral force towards the non-seam side and undergoes RS. After travelling approximately 13 m down the pitch, it slows down enough to get into the regime of CS and encounters a change in the direction of lateral aerodynamic force; it now acts in the direction of seam. This causes it to undergo CS for the remaining duration of its flight. A near 10 % decrease in the streamwise speed of the ball enables the switch from the RS to CS regime, leading

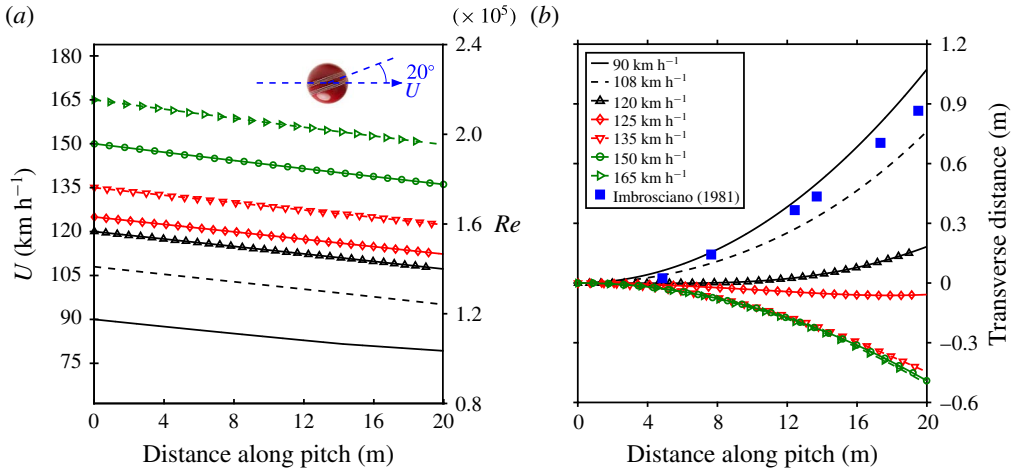

FIGURE 19. (Colour online) Variation of the (*a*) streamwise speed and (*b*) lateral deviation of the ball as it moves along the pitch length. The estimates are for a ball delivered at different initial speeds. In all cases it is assumed that the ball maintains a seam angle of $\phi_T = 20°$. Also shown in (*b*) is the lateral deviation measured by Imbrosciano (1981) for a ball delivered at 108 km h^{-1}.

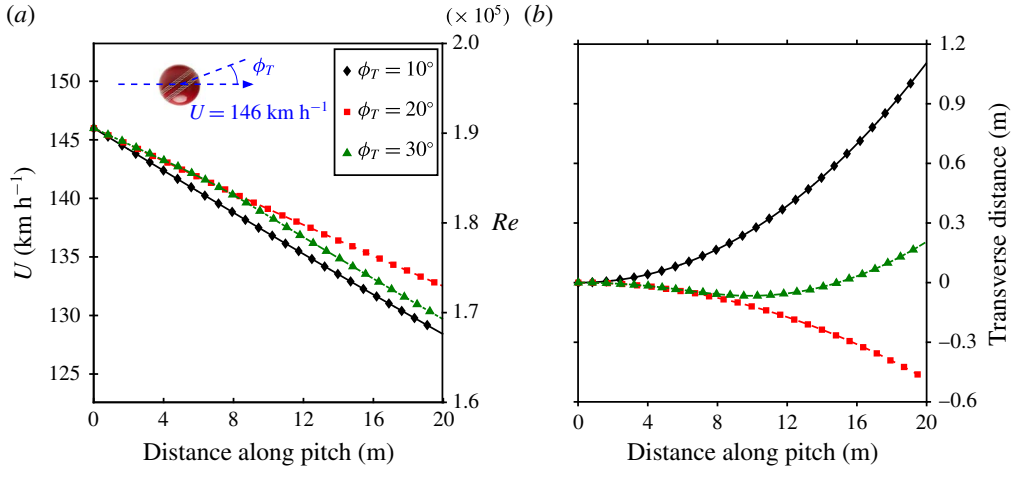

FIGURE 20. (Colour online) Variation of the (*a*) streamwise speed and (*b*) lateral deviation of the ball as it moves along the pitch length for various seam angles (ϕ_T). The initial speed of the ball is 146 km h^{-1}.

to such a trajectory. A similar trajectory may be observed for all seam orientations, albeit at different speeds of the delivery of the ball. Such trajectories have also been reported by Baker (2010) for an old/rough cricket ball.

An important parameter is the effective lateral movement of the ball between the time it is released from one end of the pitch to that when it reaches the other end. Figure 21 shows the variation of the lateral deflection of the ball with its initial speed for $\phi_T = 20°$. The ball does not undergo any lateral movement when it is delivered at speeds lower than approximately 30 km h^{-1}. It exhibits CS for 30–119 km h^{-1}

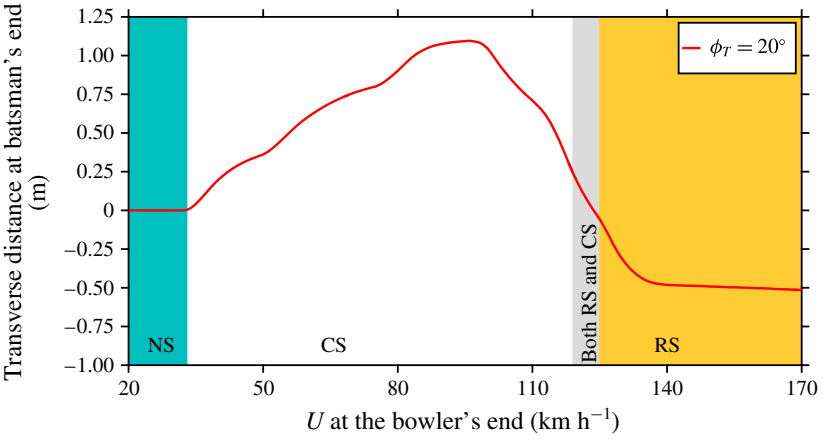

FIGURE 21. (Colour online) The lateral deviation of the ball when it reaches the end of the pitch for various speeds at the time of its delivery. In all cases it is assumed that the ball maintains a seam angle of $\phi_T = 20°$.

and RS for >125 km h^{-1}. The ball exhibits both RS and CS when delivered in the speed range 119–125 km h^{-1}. This speed range has also been marked in figure 21. The speeds for the onset of CS and RS for a new cricket ball, in the present study, are slightly lower than those observed by Mehta (2005). This is possibly due to the different brand of cricket balls used in the two studies. The deliveries which undergo both RS and CS correspond to the velocity range where the lateral force C_Z reverses direction (figure 17) with decrease in speed. The trajectory of the ball for two such speeds (120 and 125 km h^{-1}) lying within this narrow band are shown in figure 19(*b*). The delivery bowled at 120 km h^{-1} undergoes a 'late' swing. The lateral force on the ball, in the initial stage of its trajectory, is very low (figure 17). With decrease in its speed of the order of 10 % (figure 19*a*), the flow switches from RS to CS, resulting in a significantly larger swing force during the later part of its trajectory. Although, the net lateral displacement of the ball is relatively low in this regime, it is particularly difficult for the batsman to anticipate such a trajectory of the ball.

3.9.2. *Rough cricket ball*

Trajectory analysis is carried out for the models S–R, NS–R and C–R for $\phi_T = 20°$ using the data for aerodynamic forces acting on the ball presented in figure 18. Figure 22 shows the variation, with its initial speed, of the lateral deflection of the ball, at the far end of the pitch. Also shown is the deflection for a new ball. The speed for the onset of CS is lowest for S–R and C–R models and largest for the NS–R model. The peak lateral deflection during CS is largest for the new ball and lowest for the completely rough (C–R) ball. Interestingly, the initial speed of the ball that leads to peak deflection during CS is lowest for C–R, followed by NS–R, S–R and new ball. An interesting point brought out by figure 22 is that the speed of delivery of the ball that achieves maximum lateral movement, during CS, depends on the condition of the ball. A fast bowler would be an ideal choice with a new ball; a relatively slower bowler would achieve CS more effectively with a completely roughened ball (C–R). It is noted that the NS–R and C–R models exhibit CS for two ranges of speeds. The deflection in the higher range of speeds is significantly smaller than in the lower range.

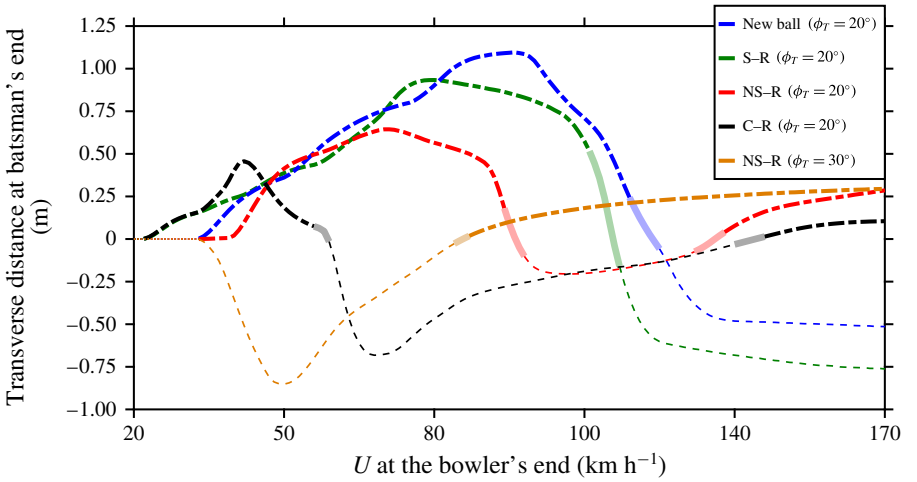

FIGURE 22. (Colour online) The lateral deviation of the ball when it reaches the end of the pitch for various initial speeds. The thick dashed lines represent CS while the thin dashed lines show the speed range where the ball experiences RS. The speed range corresponding to the deliveries that exhibit both RS and CS during their flight is highlighted by a thicker shaded line for each configuration. The speed range for the NS regime is shown as a dotted line.

Both new and C–R balls lead to comparable peak lateral movement during RS, although at different speeds. The new ball reverses at very high speed while the C–R model exhibits similar RS at relatively low speed. The range of initial speed that leads to RS for various models at $\phi_T = 20°$ is 59–141 km h^{-1} for C–R, 98–133 km h^{-1} for NS–R, >117 km h^{-1} for S–R and >125 km h^{-1} for the new ball. The lowest speed for the ball to undergo RS is smallest for C–R, followed by NS–R, S–R and a new ball.

The deliveries that exhibit both RS and CS, for a new ball (119–125 km h^{-1}) as well as S–R model (111–117 km h^{-1}), occur in a very narrow and comparable range of initial speed. Interestingly, for the NS–R and C–R models (at $\phi_T = 20°$), similar trajectories can occur in two ranges of speed. For example, for the NS–R model, the ball first moves away from the seam and then towards the seam when delivered in the speed range 94–98 km h^{-1}. It will exhibit both CS and RS again when delivered in the speed range 133–138 km h^{-1}. However, this time the nature of deflection is the reverse of the former; the ball initially moves towards the seam and after it has slowed down it moves away from the seam. The range of speeds for similar trajectories of the C–R ball is 56–59 km h^{-1} and 141–146 km h^{-1}, respectively. An interesting observation from figure 22 is that the lateral movement for the C–R ball is relatively small when delivered at a speed in excess of 120 km h^{-1}. Figure 22 also shows the variation, with speed, of the lateral deflection of the NS–R ball at $\phi_T = 30°$. This variation is starkly different compared to that at $\phi_T = 20°$. For $\phi_T = 30°$, the roughness of the non-seam side leads to a direct transition from NS to RS at fairly low *Re*. The transition to CS occurs on further increasing the speed.

4. Conclusions

The role of the seam in the swing of a cricket ball has been investigated via unsteady force and surface-pressure measurements and oil-flow visualization.

Experiments have been carried out for various speeds of the non-spinning ball and for several orientations of its seam to the flow. It is found that the seam has no significant effect on the flow up to a certain *Re*. Consequently, there is no appreciable lateral force on the ball in this regime and this is referred to as NS. Beyond a certain critical *Re*, the perturbations to the flow from the seam trigger the transition of the boundary layer on the seam side of the ball while the undisturbed flow on the non-seam side continues to remain laminar. The flow on this side is very similar to the subcritical flow over a smooth sphere. An LSB forms on the seam side in the region $-60^\circ < \theta < 60^\circ$. In the region where the seam is closer to the shoulder of the ball, the flow either directly transitions to a turbulent state on encountering the seam ($60^\circ < \theta < 80^\circ$ and $-80^\circ < \theta < -60^\circ$), or fully separates without reattaching at a downstream location ($80^\circ < \theta < 90^\circ$ and $-90^\circ < \theta < -80^\circ$). The asymmetry in the flow, between the seam and non-seam sides, generates a lateral force on the ball causing it to deviate towards the seam side. This is referred to as conventional swing (CS). The extent of the region occupied by the LSB reduces, in both polar and azimuthal directions, with increase in *Re*. The LSB completely disappears from the seam side towards the end of the CS regime. With further increase in *Re* beyond a certain value, the boundary layer on the non-seam side also transitions to a turbulent state accompanied by the formation of an LSB. In this regime the ball experiences a lateral force away from the seam. This is referred to as RS. The reversal of the swing force (from CS to RS) is accompanied by an abrupt decrease in the mean drag coefficient, again pointing to the transition of the flow on the non-seam side. The present study, therefore, clearly shows that the major cause for the RS of a new cricket ball is the transition of the boundary layer on its non-seam side.

Interestingly, the lateral force coefficient acquires a constant value in each of the fully developed CS ($\sim$0.35) and RS (~ -0.15) regimes. This is despite the variation of the extent of the LSB (during CS) with *Re*. Additionally, these values appear to be independent of the models used in the study. Analysis of the data from surface-pressure measurements reveals that, in the CS, the difference in the suction between the seam and non-seam sides, just downstream of the shoulder ($90^\circ < \phi < 120^\circ$), increases with increase in *Re*. The gain in the coefficient of lateral force due to this increase is compensated by the decrease in the difference in the suction between the seam and non-seam sides for $135^\circ < \phi < 155^\circ$. During the RS regime, the pressure asymmetry between the seam and non-seam sides is mostly restricted to the azimuthal region occupied by the LSB on the non-seam side. Consequently, compared to the CS regime, the asymmetry of the flow between the seam and non-seam sides is relatively smaller in the RS regime. Owing to the circulation associated with the swing force on the ball, the flow on the seam side also changes in the RS regime. The separation of the turbulent boundary layer, on the seam side, moves upstream from $\phi \approx 135^\circ$ in the CS regime to $\phi \approx 125^\circ$ in the RS regime and is accompanied by a decrease in the peak suction. The net circulation around the ball responsible for generating the lateral force on it influences the pressure distribution and flow separation on both halves. As a result, the flow transition on the non-seam side occurs at different *Re* for various seam configurations on a sphere with trip(s) (figure 7). This observation implies that the transition on the non-seam side is affected by the flow on the seam side.

The transitions from NS to CS and from CS to RS are found to be intermittent. This is attributed to the intermittent appearance of the LSB at the transition, similar to that reported during the transition of the boundary layer on a smooth sphere (Deshpande *et al.* 2017). The LSB on the seam side appears intermittently at the onset of the CS. Similarly, the LSB on the non-seam side is intermittent at the onset

of RS. Compared to the NS–CS transition, the CS–RS transition is rather abrupt and also more interesting. Conditional time averaging of the instantaneous pressure on the surface of the ball over the two states shows an LSB on the non-seam side for the time duration when the flow is in the RS regime. No signature of an LSB is observed on the non-seam side in the conditional time-averaged pressure distribution for the CS state. The conditional time-averaged flow for the RS state also exhibits a significantly delayed final flow separation on the non-seam side and a relatively early flow separation on the seam side.

The aerodynamic force on a new SG Test cricket ball, measured from the present wind-tunnel tests, is utilized to compute its trajectory via time integration of the equations of motion. Various speeds of the ball and its seam orientation at the time of delivery by the bowler are considered. The various trajectories can be broadly classified as: no swing (NS), conventional swing (CS) and reverse swing (RS). For the CS, the maximum lateral deflection of the ball is found to be $\approx$1.1 m. It occurs when the ball is delivered at a speed of approximately 90 km h^{-1} with a seam inclination angle of $\phi_T = 20^\circ$. Interestingly, the optimal delivery speed, for maximum lateral deflection of the ball towards the seam, is not the highest speed at which CS is observed. The flight time is relatively shorter at larger speeds, giving the ball less time to swing. The lateral movement of the ball in the regime of RS is nearly 0.5 m, if it is delivered at a speed above a certain threshold value. This threshold value is found to be nearly 135 km h^{-1} for the case of $\phi_T = 20^\circ$. The analysis also reveals an interesting trajectory, when the ball is delivered in a narrow range of speed, wherein the lateral force undergoes a switch in its direction (say from RS to CS) during the flight of the ball. The ball experiences a reverse swing in the initial phase of its trajectory. With decrease in its speed, as it travels down along the pitch, the lateral force switches direction towards the seam. Consequently, the ball exhibits CS in the later part of its trajectory.

The aerodynamics of a cricket ball is very complex. The aerodynamic forces on it affect its lateral movement and depend on a variety of parameters and features of the ball. For a new cricket ball, these include the seam, surface roughness due to embossment marks, asymmetries due to fabrication, the speed at which the ball is delivered by the bowler, spin rate, axis of spin and weather conditions. With usage, the surface roughness of the ball increases and its seam begins to wear off. This complicates the situation further. To this extent, experiments have been conducted for a cricket ball that models the wear of its surface and seam after it has been used in a game for approximately 40 overs. Four sets of force measurements have been conducted: (a) new ball; (b) S–R, the seam side of the ball (and the seam) is roughened while the other half is new; (c) NS–R, the same model is mounted in the tunnel so that the non-seam side (and the seam) is rough while the other half is shiny; and (d) C–R, a completely roughened ball. The measurements bring out the relative effect of the roughness and seam on the transition of the boundary layer. The data from force measurements are utilized to carry out trajectory analysis. It is found that, compared to a new ball, the C–R model leads to the onset of CS and RS at significantly lower speed of delivery. However, the peak lateral deflection is lower during CS; it is of comparable magnitude during RS. The peak magnitude of the swing force coefficient also changes significantly as the ball becomes rougher. It decreases in the case of CS, while it increases for the case of RS, for an old ball in comparison to that observed for a new ball. In almost all cases, the ball first undergoes CS as the speed of the delivery is increased, followed by RS at higher speed. The case of model NS–R and $\phi_T = 30^\circ$ is very interesting. Unlike for a new ball, for this model,

the roughness of the non-seam side leads to a transition of the flow at a fairly low *Re*, causing the ball to experience a lateral force away from the seam (RS). The force changes direction, towards the seam (CS), at larger *Re*. Thus, the surface roughness and the seam orientation of the ball can be suitably used by the bowler to control the lateral movement of the ball.

The models tested in the present study span an entire range of surface roughness. The two ends of the spectrum are (i) a completely roughened cricket ball (C–R) and (ii) an idealized model of a new cricket ball, i.e. a smooth sphere with trip(s). Figure 7 shows that the variation of the force coefficients with *Re* is qualitatively very similar for the new cricket ball and a smooth sphere with trip(s). The peak force coefficients achieved during CS and RS regimes are also very similar for all the models. Figure 16 shows that transition from CS to RS for the C–R cricket ball is also similar to the new cricket ball. However, there are some differences. The critical *Re* for the transition is lower for the C–R ball. Also, the peak lateral force during CS is smaller while that during RS is relatively larger for the C–R ball, compared to that for a new ball. It is also observed from figures 7 and 16 that the range of *Re* for which the CS regime persists decreases with increased surface roughness of the model. In view of these observations, a question arises: How well do the flow mechanisms gleaned from experiments with the model of a sphere with trip(s) extend to that for a new cricket ball? A new cricket ball may be considered as a part of a continuum between a sphere with trip(s) and a completely roughened (C–R) cricket ball. Therefore, the exact flow phenomena over a new cricket ball may, in principle, vary from what is observed on a sphere with trip(s). Although it cannot be established without conducting flow diagnostics for the actual cricket ball, we surmise that the flow mechanisms are very similar. However, the range of *Re* for which the LSB persists during the various regimes decreases with increase in roughness of the surface.

The present study is limited in the sense that it does not consider the effect of deformation of the ball as the game progresses. Further, the distribution of surface roughness is not expected to be uniform across the ball, as has been modelled in the present study. The present study also does not address the effect of the rotation on the swing of the cricket ball. Indeed, the rotation of the ball influences the swing force coefficient significantly (Barton 1982), which in turn influences its trajectory in terms of its lateral movement. Barton (1982) attributed this to the strong influence of the various surface irregularities on the transition of the boundary layer on the rotating surface of the ball. The present study focuses on the role of the seam in the generation of pressure asymmetry leading to lateral force, and does not address the rotation of the ball. It is quite likely that the flow phenomena for an actual cricket ball in play might be modified by the added perturbation from the embossment marks and surface roughness on a rotating ball (Barton 1982). Hence, the quantitative analysis presented in the study may not exactly represent that in actual play. It would be interesting to further explore these effects via a systematic variation of the parameters. Investigation into the aerodynamics of a rotating ball will also bring to the fore the vertical trajectory of the ball, wherein the forces due to the Magnus/inverse Magnus effect augment the force due to gravity.

Acknowledgements

The authors would like to acknowledge Mr Sharad Saxena, Mr Vivek Kanti and Mr Akhilesh Pal of the National Wind Tunnel Facility, IIT Kanpur, for their help

in conducting the experiments. They are grateful to Professors Alakesh Chandra Mandal and Kamal Poddar for making available some of their facilities for carrying out the experiments and to Dr Navrose and Mr Aditya Desai for their enthusiastic participation in the discussions related to the analysis of the experimental data. The authors are also grateful to the anonymous reviewers for their insightful suggestions.

REFERENCES

ACHENBACH, E. 1972 Experiments on the flow past spheres at very high Reynolds numbers. *J. Fluid Mech.* **54** (03), 565–575.

ACHENBACH, E. 1974 The effects of surface roughness and tunnel blockage on the flow past spheres. *J. Fluid Mech.* **65** (01), 113–125.

ANDERSON, J. D. 1991 *Fundamentals of Aerodynamics*. McGraw-Hill.

BAKER, C. J. 2010 A calculation of cricket ball trajectories. *Proc. Inst. Mech. Engrs* C **224** (9), 1947–1958.

BARTON, N. G. 1982 On the swing of a cricket ball in flight. *Proc. R. Soc. London* A **379**, 109–131.

BENTLEY, K., VARTY, P., PROUDLOVE, M. & MEHTA, R. D. 1982 An experimental study of cricket ball swing. Aero Tech. Note, Imperial College, pp. 82–106.

CADOT, O., DESAI, A., MITTAL, S., SAXENA, S. & CHANDRA, B. 2015 Statistics and dynamics of the boundary layer reattachments during the drag crisis transitions of a circular cylinder. *Phys. Fluids* **27** (1), 014101.

DESHPANDE, R., KANTI, V., DESAI, A. & MITTAL, S. 2017 Intermittency of laminar separation bubble on a sphere during drag crisis. *J. Fluid Mech.* **812**, 815–840.

IGARASHI, T. 1986 Effect of tripping wires on the flow around a circular cylinder normal to an airstream. *Bull. JSME* **29** (255), 2917–2924.

IMBROSCIANO, A. 1981 The swing of a cricket ball. Proj. Rep. 810714, Newcastle College of Advanced Education.

KIM, J., CHOI, H., PARK, H. & YOO, J. Y. 2014 Inverse Magnus effect on a rotating sphere: when and why. *J. Fluid Mech.* **754**, R2.

MAXWORTHY, T. 1969 Experiments on the flow around a sphere at high Reynolds numbers. *Trans. ASME J. Appl. Mech.* **36** (3), 598–607.

MEHTA, R. D. 1985 Aerodynamics of sports balls. *Annu. Rev. Fluid Mech.* **17** (1), 151–189.

MEHTA, R. D. 2005 An overview of cricket ball swing. *Sports Engng* **8** (4), 181–192.

MEHTA, R. D. 2014 Fluid Mechanics of Cricket Ball Swing. In *19th Australasian Fluid Mechanics Conference*.

MEHTA, R. D., BENTLEY, K., PROUDLOVE, M. & VARTY, P. 1983 Factors affecting cricket ball swing. *Nature* **303**, 787–788.

NORMAN, A. K., KERRIGAN, E. C. & MCKEON, B. J. 2011 The effect of small-amplitude time-dependent changes to the surface morphology of a sphere. *J. Fluid Mech.* **675**, 268–296.

NORMAN, A. K. & MCKEON, B. J. 2008 Effect of sting size on the wake of a sphere at subcritical Reynolds numbers. In *AIAA 8th Fluid Dyn. Conf. and Exhibit.* AIAA 2008-4237.

NORMAN, A. K. & MCKEON, B. J. 2011 Unsteady force measurements in sphere flow from subcritical to supercritical Reynolds numbers. *Exp. Fluids* **51** (5), 1439–1453.

SCOBIE, J. A., PICKERING, S. G., ALMOND, D. P. & LOCK, G. D. 2012 Fluid dynamics of cricket ball swing. *Proc. Inst. Mech. Engrs* P **227** (3), 196–208.

SHERWIN, K. & SPROSTON, J. L. 1982 Aerodynamics of a cricket ball. *Int. J. Mech. Educ* **10** (7), 1–79.

SINGH, S. P. & MITTAL, S. 2005 Flow past a cylinder: shear layer instability and drag crisis. *Intl J. Numer. Meth. Fluids* **47** (1), 75–98.

SON, K., CHOI, J., JEON, W.-P. & CHOI, H. 2010 Effect of free-stream turbulence on the flow over a sphere. *Phys. Fluids* **22** (4), 045101.

SON, K., CHOI, J., JEON, W.-P. & CHOI, H. 2011 Mechanism of drag reduction by a surface trip wire on a sphere. *J. Fluid Mech.* **672**, 411–427.

SURYANARAYANA, G. K., PAUER, H. & MEIER, G. E. A. 1993 Bluff-body drag reduction by passive ventilation. *Exp. Fluids* **16** (2), 73–81.

SURYANARAYANA, G. K. & PRABHU, A. 2000 Effect of natural ventilation on the boundary layer separation and near-wake vortex shedding characteristics of a sphere. *Exp. Fluids* **29** (6), 582–591.

TANEDA, S. 1978 Visual observations of the flow past a sphere at Reynolds numbers between 10^4 and 10^6. *J. Fluid Mech.* **85** (01), 187–192.

WIESELSBERGER, C. 1914 Der luftwiderstand von kugeln. *Z. Flugtechnik Motorluftschiffahrt* **5**, 140–145.

WIESELSBERGER, C. 1922 Neuere feststellungen über die gesetze des flüssigkeits- und luftwiderstandes. *Phys. Z.* **22** (11), 321–328.